TÉCNICO LISBOA

Development of methods for material properties identification in composite structures

André Filipe Ferreira Rodrigues

Thesis to obtain the Master of Science Degree in

Aerospace Engineering

Supervisor: Prof. José Viriato Araújo dos Santos

Examination Committee

Chairperson: Prof. Filipe Szolnoky Ramos Pinto Cunha
Supervisor: Prof. José Viriato Araújo dos Santos
Member of the Committee: Prof. Aurélio Lima Araújo

January 2021

This master's thesis is dedicated to my family, specially to my parents and my godmother that supported me through this arduous route.

Declaration

I declare that this document is an original work of my own authorship and that it fulfills all the requirements of the Code of Conduct and Good Practices of the Universidade de Lisboa.

Acknowledgments

First and foremost, I would like to thank my advisor Professor José Viriato Araújo dos Santos for all guidance and advice given during this thesis. His guidance was fundamental to the development and writing of this thesis. I would also like to thank Professor Hernâni Miguel Reis Lopes from ISEP for providing experimental data used during this work.

A special thanks to my friends from Lisbon and Viseu, which helped me develop this thesis by lending me their computers and rereading this document over and over.

To my family, a very special thank you for all the love and care. To my parents, who always have supported me, to my godmother, who always encouraged me, and to my grandparents.

Finally, I would like to thank my girlfriend for always being there when a word of encouragement and motivation was needed.

Resumo

Esta tese de mestrado propõe um método não destrutivo para a identificação de propriedades de materiais compósitos utilizando softwares comerciais, nomeadamente ANSYS® e MATLAB®.

O método proposto tira partido das capacidades de simulação do ANSYS®, usando ANSYS® Parametric Design Languague (APDL), para a realização de análises modais e extrair frequências naturais dos espécimes. O ANSYS® e o MATLAB® são integrados para resolverem os vários problemas de otimização. Os problemas de otimização propostos têm como variáveis de design as constantes elásticas do material e usam algoritmos de otimização meta heurísticos inspirados na Natureza. Estes avaliam uma função objetivo, cujo intuito é relacionar frequências naturais experimentais, extraídas de alguns estudos realizados por outros autores, com frequências naturais obtidas computacionalmente, e sem necessidade do cálculo de derivadas.

Os algoritmos meta heurísticos de otimização inspirados na Natureza testados foram o Genetic Algorithm, o Particle Swarm Optimisation Algorithm, o Grey Wolf Optimisation Algorithm, o Firefly Algorithm e o Cuckoo Search Algorithm. As diferentes populações de agentes de pesquisa gerados pelos algoritmos percorrem o espaço de procura de modo a localizarem o mínimo global da função, independentemente da distribuição da população no espaço de pesquisa. O método proposto é aplicado a vários espécimes de diferentes materiais, quer eles sejam construídos com fibras sintéticas, como fibras de vidro, ou fibras naturais, como fibras de madeira e contraplacado.

Em suma, este método demonstrou obter as constantes elásticas dos materiais dentro num intervalo aceitável quando comparado com métodos alternativos, desde que sejam medidas com precisão e fornecidas frequências naturais suficientes.

Palavras-chave: Materiais compósitos, Compósitos verdes, Propriedades dos materais, Constantes elásticas, Optimização inspirada na Natureza

Abstract

This master thesis proposes a non-destructive method for the identification of material properties of composite materials. This method takes advantage of the simulation capabilities of ANSYS® software, using ANSYS®Parametric Design Language (APDL) to perform modal analyses and extract natural frequencies of the specimens.

ANSYS® and MATLAB® are integrated to solve several optimisation problems. The proposed optimisation problems have for design variables the material elastic constants and make use of Nature-inspired metaheuristic optimisation algorithms to evaluate an objective function using a derivative-free method. These objective functions relate experimental natural frequencies, which are extracted from numerous studies carried out in the past by other authors, with computationally obtained ones. The Nature-inspired metaheuristic optimisation algorithms tested are the Genetic algorithm, the Particle Swarm Optimisation algorithm, the Grey Wolf Optimisation algorithm, the Firefly Algorithm and Cuckoo Search algorithm. The different search agents population generated by the algorithms search the available space looking for the global minimum of the objective function, independently of the initial population position in the search space.

The proposed method is applied to several specimens of different materials either they are constructed with synthetic fibres, such as glass fibres, or natural fibres, such as wood fibres and plywood. This method proved to obtain the material elastic constants within an acceptable range, compared to other methods, provided that enough natural frequencies are accurately measured and provided.

Keywords: Composite Materials, Green composites, Material Properties, Elastic constants, Nature-inspired optimisation

Contents

List of Tables

List of Figures

Nomenclature

Greek symbols

ν_{12}, ν_{21} Poisson ratio

ω_i Computational natural circular frequencies

Φ Objective function

ϕ Mode shape function

Φ_1, Φ_2 and Φ_3 Objective functions

ρ Density

σ Stress

$\tilde{\omega_i}$ Experimental natural circular frequencies

ε Strain

Roman symbols

$\tilde{fr_i}, \tilde{f_{Bx}}, \tilde{f_{By}}, \tilde{f_T}, \tilde{f_+}, \tilde{f_H}, \tilde{f_L}, \tilde{f_O}, \tilde{f_X}$ Experimental natural frequencies

a Length

a_e Element dimension

b Width

C_{ij} Stiffness coefficient

D_1, D_2, D_3, D_4 Equivalent elastic constants

E_1, E_2, E_3 Young's modulus of the three principal directions of the material

f_i Natural frequency

$fr_i, f_{Bx}, f_{By}, f_T$ Computational natural frequencies

G_{12}, G_{13}, G_{23} Shear modulus in each of the three principal directions

h Thickness

MCI	Mesh convergence index
nf	Number of frequencies
S_{ij}	Compliance coefficient
t	Time
u	Displacement in the x direction
v	Displacement in the y direction
W_i	Weight factor
x, y, z	Direction components in a Cartesian system
Fval	Function values
NFEs	Number of function evaluations
Niter	Number of iterations
RCTime	Relative computational time

Glossary

APDL ANSYS Parametric Design Language. 21

CS Cuckoo Search. 18

FA Firefly Algorithm. 17

FEM Finite Element Method. 5

GA Genetic Algorithm. 8

GWO Grey Wolf Optimizer. 16

NPL National Physics Laboratory. 7

OSB Composite material composed of adhesive and wooden strands. 22

PSO Particle Swarm Optimization. 8

Chapter 1

Introduction

The urge of the automotive and aerospace industries to develop new lighter vehicles with a smaller biological blueprint boosted the development of new materials. The search for new materials has been one of the major focus points of engineers over the last years. These new materials have better mechanical properties than the existing ones. To achieve this, engineers developed what is known as composite materials.

These new composite materials are tailored to the specific need of each project. The most common used materials in composites are carbon fibres, glass fibres and aramid fibres, that are obtained from non-renewable sources. Therefore, searching for sources of renewable materials is essential; materials like wood, jute straw and flax can easily be processed into natural fibres that are transformed in what is called green composites.

Green composites or natural fibre composites are the combination of natural fibres with a polymeric matrix; this allows the use of several combinations of materials to achieve the desired properties.

In a case study presented in 2010, Alves et al. investigated in a case study the replacement of glass fibres for natural jute fibres, producing a structural front bonnet of an off-road vehicle [1]. This replacement has proven to enhance the environmental performance of the vehicle, reducing weight and therefore, fuel consumption. More recently, several automotive companies, in the motorsports industry, have replaced some body components with natural fibres composites. The first example of the replacement of carbon fibres with natural fibres in serial production for motorsports was performed by Porsche®, which replaced doors with balsa wood as the core of a composite sandwich material and in collaboration with Composites Evolution Ltd and KW Special Projects Ltd replaced the rear wing, previously constructed with carbon fibres, with flax fibres impregnated with epoxy resin (Figure 1.1) [2].

More recently, the automotive industries are starting to integrate these materials in components, such as in car seat backs using a hybrid carbon and wood fibre to develop a lightweight carbon fibre prepreg and wood fibre composite part, obtaining a forty percent reduction of the weight compared to the standard injection moulded plastic, resulting in a significant improvement in the CO_2 footprint [3]. At the Nürburgring 24-hour race, Porsche® presented a complete body kit made of natural fibre composite materials for the first time, Figure 1.2(a). Not only the doors and rear wing materials were replaced, but

Figure 1.1: Rear wing constructed with flax fibres and epoxy resin [2]

also, for the first time, the front and rear aprons, Figure 1.2(b), the front spoiler, the front and rear lids, the mudguards and the diffuser materials were replaced with natural fibre composites. This composite is composed of flax fibres, farmed without conflicting with food crops, layered up with a polymeric matrix to ensure the precise adjustment to specific purposes and load scenarios [4]. These natural fibre composite

((a)) Porsche 718 Cayman GT4 Clubsport MR natural fibres body

((b)) Flax fibres epoxy resin rear apron

Figure 1.2: Images extracted from Porsche's newsroom [4]

materials have proven to be particularly suited to areas that are not part of the main vehicle structure. Moreover, the damping of vibrations improves fivefold and, in the case of an accident, splinter into larger and less sharp pieces [4].

1.1 Topic Overview

The use of composite materials in these last decades has grown exponentially, mainly in the transport industries, such as aircraft, aerospace, automotive, naval and much more. This is due to the possibility of having materials engineered to a specification, including requested mechanical properties and complex shapes.

Composite materials are the result of the combination of two or more different materials, as they can be the combination of metals and ceramics, metals and polymers or even ceramics and polymers, as represented in Figure 1.3. These can be natural or man-made regarding their origin. Natural composite

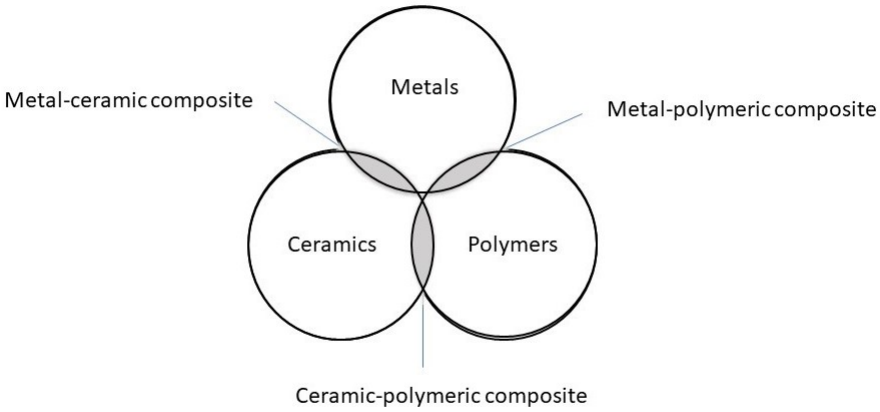

Figure 1.3: Representative diagram with the 3 basic materials and the composite materials [5]

materials such as bones and wood are materials that appear in nature. Bones are a naturally occurring composite material having within its structure calcium phosphate (mineral) embedded in a collagen (protein) matrix. The same goes for wood having within its structure cellulose fibres bonded with a polymeric substance (lignin).

Man-made composite materials are developed, in order to obtain stronger, lighter, heat resistant or electric insulating materials. These materials have new properties that could not be achieved by the constituent materials themselves. One of the earliest records of a Man-made composite is mud bricks. These bricks are the combination of straw and mud, having been used for construction since primitive times.

The characteristic structure of a Man-made composite material is formed by a matrix (binder material) and a reinforcement material. The reinforcement material can be added to the structure in different forms such as powder, short fibres (discontinuous fibres) and long fibres (continuous fibres). The most commonly used reinforcement in composite materials is fibre reinforcement. Reinforcement fibres can be characterised based on their origin, being synthetic fibres or natural fibres. Nowadays, in the industry, the use of synthetic fibres is generalised, with the most used being carbon fibres, glass fibres and aramid

fibres.

Natural fibre-reinforced polymer composites have attracted more and more research interests owing to their potential as an alternative for synthetic fibre composites. Natural fibre composites possess advantages such as easy availability, renewability of raw materials, low cost, lightweight, high specific strength and stiffness.

Application of natural fibres, from sustainable sources, has substantially increased in recent years. The use of natural fibres in composites was investigated and analysed by Saxena et al. [6]. The natural fibres investigated were flax, hemp, jute straw, wood, rice husk, wheat, barley, oats, rye, cane (sugar and bamboo), grass reeds, kenaf, ramie, oil palm, sisal, coir, water hyacinth, pennywort, kapok, paper mulberry, banana fibre, pineapple leaf fibre and papyrus. The use of natural fibre reinforced composite materials for the automotive industries has been studied and reviewed by Koronis et al. [7], defining them as green composites. Green composites are composite materials derived from renewable and sustainable sources, being the combination, most of the times, of a polymeric matrix and natural fibre as reinforcement. The benefit of using natural fibre composite materials revolve around environmental sustainability, which includes reduced carbon footprint, biodegradability and renewability. However, there are other direct benefits to such as light weight, high specific properties, good thermal insulation and vibration damping.

The most used structure of a Man-made composite material is a layered internal structure, being characterised as laminated composite, where the layered material is arranged in different directions to obtain the desired properties. In this case, the reinforced material is used in a weaved form, making the construction of the final composite material simpler, allowing for a uniform fibre arrangement in the desired direction.

1.2 Objectives

During the design of structures or structural components, materials with specific properties are needed. Therefore, new composite materials are created in order to meet design requirements. As a consequence, it is imperative to assess the mechanical properties of these composite materials. Taking into account that composite materials are heterogeneous by nature, in order to fully determine all the mechanical properties, it is necessary to perform a vast number of tests, which have a cost. In this thesis, a non-destructive method for properties identification is developed. It relies on commercial software to easily obtain an estimation of the mechanical properties of the specimen in the study. Nature-inspired optimisation algorithms are used in order to minimise an error function relating experimental and computational modal parameters.

This thesis focuses on the study of laminated composite materials, whether they are synthetic fibre reinforced, such as glass fibres reinforced specimens, or they are natural fibres reinforced like wooden fibres reinforced composites and plywood. However, a specimen of aluminium is also analysed to establish a baseline and test the proposed method.

1.3 Thesis Outline

In chapter two is presented a brief overview of metaheuristic optimisation algorithms, in particular, nature-inspired optimisation algorithms. Also presented are methodologies for material properties identification, using non destructive testing methods. In this chapter, are also introduced and described the selected optimisation algorithms that will be tested in the present method for material properties identification.

Chapter three introduces the proposed method for material properties identification. It starts with the presentation of the specimen selected to test and analyse the method, followed by the selection of the models of each specimen, including the mesh needed for the Finite Element Method (FEM) analysis. Then, the optimisation problems are presented, where the material elastic constants correspond to the design variables of these problems. Here the proposed optimisation problems are fully defined being presented the objective function of the problems, the design variables constraints and the termination criteria.

In the next section, section 3.4, are presented the optimisation problems results and analysis of the different tests performed with this method. Firstly, the most appropriate nature-inspired optimisation algorithm to solve the problem is selected, comparing the results with those found in the literature [8, 9]. Next, a validation test is performed comparing several runs of the same problem. The next subsection is comprised of the study of several factors that influence the performance of the method, such as the objective function, the number of experimental natural frequencies and the number of search agents. In subsection 3.4.6, the proposed method for properties identification is applied to two specimens of green composites. Chapter four presents the conclusions and recommendations for future works.

Chapter 2

Theoretical and Applications Background

2.1 Historical Overview

An interesting and simple way to describe heuristic and metaheuristic methods is presented by Yang in 2010 [10].

> *"Throughout history, especially at early periods of human history, we humans' approach to problem-solving has always been heuristic or meta-heuristic – by trial and error. Many important discoveries were done by 'thinking outside the box', and often by accident; that is heuristics. Archimedes's Eureka moment was a heuristic triumph. In fact, our daily learning experience (at least as a child) is dominantly heuristic."*

The first use of the metaheuristic method is difficult to pinpoint in history, although its importance is well established in the scientific community nowadays. The first documented use of heuristic algorithms was by Alan Turing during the Second World War at Bletchley Park. He developed a method that later would be called *heuristic search* [11]. Although there was no guarantee that the correct solution could be obtained it changed the course of the War. Alan Turing continued his work being recruited for the National Physics Laboratory (NPL), in the UK in 1945. There, he developed his Automatic Computing Engine. In 1948, in an NPL report on *Intelligent machinery* [11], Alan Turing summarised his innovative ideas of what is now known as machine intelligence and learning, neural networks and evolutionary algorithms.

The 1960s and the 1970s was the time for the development of metaheuristic methods. The first metaheuristic algorithm presented was called Pattern Search presented in 1961 by Hooke and Jeeves in Pittsburgh, Pennsylvania [12]. Around the same period, in 1963/1965, Rechenberg and Schwefel, at the Technical University of Berlin, developed a search technique for solving optimisation problems in aerospace engineering, named evolutionary strategy [13]. Then, in 1966, Fogel alongside Owen and Walsh developed the evolutionary programming technique, representing solutions as a finite-state

machine and randomly mutating one of these machines. These innovative ideas and methods have grown into the field of *evolutionary algorithms* and/or *evolutionary computation* [14]. In these decades, Holland and his collaborators at the University of Michigan developed the genetic algorithms. In 1962, Holland started the study of an adaptive system using crossover and recombination manipulations for modelling this system, publishing the book that summarises the development of Genetic algorithms (GA) in 1975 [15]. In 1977, Glover developed the Scatter Search algorithm [16]. During this time and the following decades, the focus was mostly in heuristic optimisation techniques such as artificial neural networks, support vector machines and other machine learning techniques.

The golden age of metaheuristic techniques development happened during the 1980s and 1990s. Initially, in 1983, Kirkpatrick, Gellat and Vecchi developed the Simulated Annealing algorithm, which is inspired by the annealing process of metals. It is a trajectory-based search algorithm, starting with an initial guess solution at a high temperature and gradually cooling the system [17]. In 1986, Glover developed the Tabu search [18]. This algorithm uses adaptative memory programming for the first time in modern metaheuristics. It uses memories of past searches to guide future search. In this same year, Farmer, Packard and Perelson presented the artificial immune systems algorithm [19]. At the end of the decade, in 1989, Bishop presented the Stochastic Diffusion Search algorithm [20], and Moscato presented Memetic algorithm [21].

In 1992, Colorni, Dorigo and Maniezzo presented a paper on optimisation and natural algorithms, describing the Ant Colony Optimisation [22]. This method is a search technique inspired by the swarm intelligence of social ants using the pheromone as a chemical messenger. During this time, several papers and books were published setting the foundations for genetic programming, originating the basis of machine learning as they are used today. In 1993, Dueck developed the Great Deluge algorithm, this algorithm resembles the simulated annealing algorithm in structure, being the main difference the acceptance rule for worse intermediate solution [23].

Later in 1995, Particle Swarm optimisation (PSO) was developed by the american social psychologist Kennedy and the engineer Eberhart. PSO is inspired by swarm intelligence of fish and birds and even by human behaviour [24]. Since the development of PSO, there have been more than twenty variants of this technique, applied to almost all areas to solve optimisation problems. From 1997 until 1998, Storn and Price developed their vector-based evolutionary algorithm, called differential evolution [25], proving to be, in some cases, better than Genetic algorithms. During the same time, Murase and Wadano presented the Photosynthetic Learning algorithm [26].

With the development of more powerful computers, more algorithms were developed. One hundred and ninety-two metaheuristic algorithms are listed by M. Almufti [55] and seventy four Nature-inspired metaheuristic algorithms by Fister et al. [56]. Some of the most peculiar algorithms presented are the Social Spider algorithm [57], the Shark smell optimisation algorithm [58], Krill Herd algorithm [49], the Shuffled Frog Leaping algorithm [59], the Farmland fertility algorithm [60], and the Great Salmon Run algorithm [61]. By focusing on Nature-inspired metaheuristic algorithms, it is possible to list some of the most cited algorithms, which are presented in Table 2.1.

Nature-inspired algorithms gained popularity in the scientific community due to their efficiency and

Table 2.1: List of most cited optimisation algorithms [27]

Algorithm	Author	Year	Reference	Citations
Genetic	Holland	1975	[15]	60000
Particle Swarm Optimisation	Eberhart and Kennedy	1995	[24]	50000
Harmony Search	Geem et al.	2001	[28]	4000
Honey-bees Mating Optimisation	Abbass	2001	[29]	400
Bacterial Foraging	Passino	2002	[30]	2500
Shuffled Frog Leaping	Eusuff and Lansey	2003	[31]	1000
Society and Civilization	Ray and Liew	2003	[32]	300
Artificial Bee Colony	Karaboga	2005	[33]	4500
Glowworm Swarm Optimisation	Kaipa and Ghose	2005	[34]	600
Big Bang-Big Crunch	Erol and Eksin	2006	[35]	600
Cat Swarm Optimisation	Chu et al.	2006	[36]	300
Invasive Weed Optimisation	Mehrabian and Lucas	2006	[37]	750
Imperialist Competitive	Atashpaz-Gargari and Lucas	2007	[38]	1500
Biogeography-Based Optimiser	Simon	2008	[39]	2000
Group Search Optimiser	He et al.	2009	[40]	500
Firefly	Yang	2009	[41]	2000
Water Cycle	Shah-Hosseini	2009	[42]	250
Cuckoo Search	Yang and Deb	2010	[43]	500
Fireworks	Tan and Zhu	2010	[44]	300
Teaching-Learning Based Optimisation	Rao et al.	2011	[45]	1000
Bat Algorithm	Yang and Gandomi	2012	[46]	600
Flower Pollination	Yang	2012	[47]	500
Fruit Fly Optimisation	Pan	2012	[48]	600
Krill Herd	Gandomi and Alavi	2012	[49]	600
Grey Wolf Optimiser	Mirjalili et al.	2014	[50]	1000
Ant Lion	Mirjalili	2015	[51]	300
Brain Storm Optimisation	Xue et al.	2012	[52]	300
Moth-flame Optimisation	Mirjalili	2015	[53]	250
Whale Optimisation	Mirjalili and Lewis	2016	[54]	250

are classified according to the criteria used. Fister et al. [56] claim that Nature-inspired algorithms can be grouped into four categories, based on where the inspiration comes from. Most of the algorithms are based on a successful characteristic of a biological system. The majority of the algorithms are biology-inspired, like the Genetic, Evolutionary and the Flower Pollination algorithms. These biology-inspired algorithms have a particular class within the algorithms that take inspiration from swarm intelligence, such as Particle Swarm optimisation, Cuckoo Search, Firefly algorithm and Ant Colony optimisation. Not all Nature-inspired algorithms have biological inspiration. Many other algorithms have been developed by using physical and chemical systems as inspiration, such as the Big Bang-Big Crunch and the Simulated Annealing algorithms.

Despite the benefits described above, Nature-inspired algorithms also have some drawbacks. These algorithms may require a large sample of objective function evaluations in order to solve the problem. This implies that a large amount of computational power may be necessary to process the data. Additionally, there is no guarantee that a global minimum is obtained, having the possibility instead of finding a local minimum.

2.2 Overview of methods for materials characterisation

Materials are characterised by their engineering constant, also known as elastic constants. Different elastic constants represent different characteristics of the structure. In this thesis, the elastic constants analysed are Young's modulus, E, which relates extensional strain in the direction of loading to stress in the direction of loading, the Poisson's ratio, ν, relates extensional strain in the loading direction to extensional strain in another direction. The shear modulus, G, relates shear strain in the plane of shear loading to that shear stress. However, there are others like the coefficient of mutual influence, which relates the shear strain due to shear stress in the plane to extensional strain, or the Chentsov coefficient which relates shear strain due to shear stress in that plane to shear strain in another plane [62].

For example for an orthotropic material, the stress-strain relations take the form:

$$\begin{Bmatrix} \sigma_1 \\ \sigma_2 \\ \sigma_3 \\ \sigma_4 \\ \sigma_5 \\ \sigma_6 \end{Bmatrix} = \begin{bmatrix} C_{11} & C_{12} & C_{13} & 0 & 0 & 0 \\ C_{12} & C_{22} & C_{23} & 0 & 0 & 0 \\ C_{13} & C_{23} & C_{33} & 0 & 0 & 0 \\ 0 & 0 & 0 & C_{44} & 0 & 0 \\ 0 & 0 & 0 & 0 & C_{55} & 0 \\ 0 & 0 & 0 & 0 & 0 & C_{66} \end{bmatrix} \begin{Bmatrix} \varepsilon_1 \\ \varepsilon_2 \\ \varepsilon_3 \\ \varepsilon_4 \\ \varepsilon_5 \\ \varepsilon_6 \end{Bmatrix} \tag{2.1}$$

where C_{ij} are the stiffness coefficients, σ_i are stresses and ε_i are strains.

Since most of the experimental tests are performed knowing the load or stress applied to a structure is convenient to write the inverse relation. In this case, the strain-stress relations for an orthotropic material takes the form:

$$\Rightarrow \begin{Bmatrix} \varepsilon_1 \\ \varepsilon_2 \\ \varepsilon_3 \\ \varepsilon_4 \\ \varepsilon_5 \\ \varepsilon_6 \end{Bmatrix} = \begin{bmatrix} S_{11} & S_{12} & S_{13} & 0 & 0 & 0 \\ S_{12} & S_{22} & S_{23} & 0 & 0 & 0 \\ S_{13} & S_{23} & S_{33} & 0 & 0 & 0 \\ 0 & 0 & 0 & S_{44} & 0 & 0 \\ 0 & 0 & 0 & 0 & S_{55} & 0 \\ 0 & 0 & 0 & 0 & 0 & S_{66} \end{bmatrix} \begin{Bmatrix} \sigma_1 \\ \sigma_2 \\ \sigma_3 \\ \sigma_4 \\ \sigma_5 \\ \sigma_6 \end{Bmatrix} \tag{2.2}$$

where S_{ij} are the compliance coefficients, ε_i are strains and σ_i are stresses.

Most of the times, the material properties are determined in a laboratory in terms of engineering constants such as Young's modulus, shear modulus and Poisson's ratio. These constants are measured using simple tests like uniaxial tension test. Due to their physical meaning, the engineering constants are used in place of more abstract stiffness coefficients and compliance coefficients. Thus the relation between strains and stresses can be written as a function of the engineering constants according to:

$$\begin{Bmatrix} \varepsilon_1 \\ \varepsilon_2 \\ \varepsilon_3 \\ \varepsilon_4 \\ \varepsilon_5 \\ \varepsilon_6 \end{Bmatrix} = \begin{bmatrix} \frac{1}{E_1} & -\frac{\nu_{21}}{E_2} & -\frac{\nu_{31}}{E_3} & 0 & 0 & 0 \\ -\frac{\nu_{12}}{E_1} & \frac{1}{E_2} & -\frac{\nu_{32}}{E_3} & 0 & 0 & 0 \\ -\frac{\nu_{13}}{E_1} & -\frac{\nu_{23}}{E_2} & \frac{1}{E_3} & 0 & 0 & 0 \\ 0 & 0 & 0 & \frac{1}{G_{23}} & 0 & 0 \\ 0 & 0 & 0 & 0 & \frac{1}{G_{13}} & 0 \\ 0 & 0 & 0 & 0 & 0 & \frac{1}{G_{12}} \end{bmatrix} \begin{Bmatrix} \sigma_1 \\ \sigma_2 \\ \sigma_3 \\ \sigma_4 \\ \sigma_5 \\ \sigma_6 \end{Bmatrix} \tag{2.3}$$

where E_1, E_2, E_3 are the Young's modulus in 1, 2, and 3 material directions, respectively, ν_{ij} is the Poisson's ratio, defined as the ratio of the transverse strain in the jth direction to the axial strain in the ith direction when stressed in the ith direction, and G_{23}, G_{13}, G_{12} are the shear moduli in the 2-3, 1-3, and 1-2 plane respectively [63].

The methods for material properties identification, and therefore engineering constants identification, can be divided into two classes: methods that use destructive techniques and non-destructive ones, as can be seen in Figure 2.1.

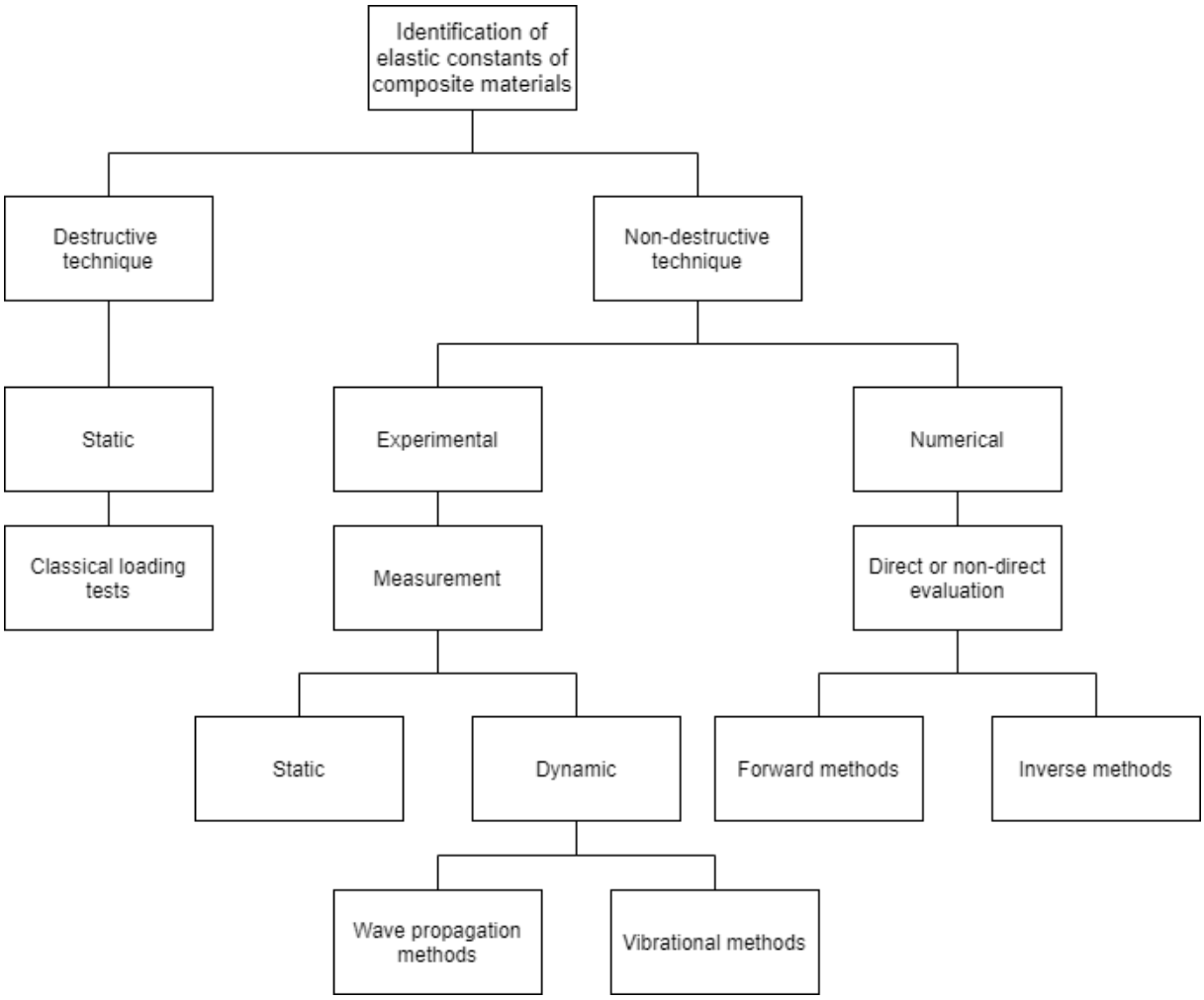

Figure 2.1: Overview of composite material properties identification methodologies [64].

The destructive techniques involve static mechanical tests, such as tensile tests, compression tests, bending tests and torsion tests. With these experimental tests one obtains the strains and stresses of

the specimen and then, using the stress-strain theory, the material elastic constants are determined.

On the other hand, non-destructive techniques involve two parts, an experimental and a numerical part, being these techniques most of the times referred to as experimental-numerical techniques [64]. In the experimental part, significant parameters are measured and extracted to be later used in the numerical part. Two approaches are considered, namely the static and the dynamic approaches. In the static approach, a specimen is subjected to a transverse quasi-static load, taking into consideration not to exceed an induced strain over 0.5%. Thus the deflection experienced during the test can fully be recovered at the end. The dynamic approach can be divided into the wave propagation method and the vibrational method. The wave propagation method uses an ultrasonic wave travelling through a specimen. This method is based on the time that the wave takes between the transducer and the receiving transducer. It presents several disadvantages, namely the formation of several waveforms in single frequency waves and the complex experimental procedure. The vibrational method makes use of external excitations in order to obtain a frequency response function and to extract from them modal parameters, in particular natural frequencies and mode shapes. The natural frequencies are the frequencies at which a physical structure will tend to vibrate. Natural frequencies are dependent on the way mass and stiffness are distributed within the structure. Each structure posses its unique set of natural frequencies and mode shapes. A mode shape describes how a structure moves at a particular natural frequency.

To fully determine the material properties of the specimens in study, the numerical part of this method can be a direct evaluation, in which the direct identification of elastic properties of a material is obtained from a derived inverse equation with the experimental resonant frequencies as data. Alternatively, it can be a non-direct evaluation, in which the objective is the minimisation or maximisation of objective functions. This last approach involves both forward methods and inverse methods in order to determine the material properties of the composite material in the study, as can be seen in Figure 2.2.

In the forward methods, parameters, such as natural frequencies or mode shapes, are evaluated using inputs of elastic properties of the material depending on the approach taken. In the inverse methods, the main objective is the minimisation of an error function that is written as a difference between experimental and evaluated constructive parameters. In the diagram (Figure 2.2), it is possible to observe the relation between the two methods.

Soares et al. [8] used the indirect method to predict material properties of composite plates. In this case, experimentally determined eigenfrequencies of the plate in the study are compared to the corresponding numerical eigenvalues through the use of an objective function, and an optimisation technique is applied. The generalisation of this method is presented by Araújo et al. [65], where experimental values of material parameters are determined, and in this case, the numerical part consists in a finite element analysis to determine the corresponding numerical eigenfrequencies. After that, it is used an optimisation technique comprised of the minimisation of an error function that estimates the deviation between experimental and numerical values.

Some years later, based on these previous articles, Lopes et al. [9] presented a method for the identification of material constants of laminated composite plates. The optimisation process makes use

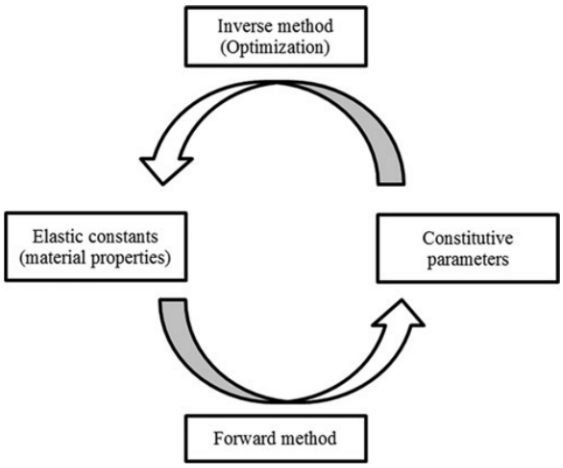

Figure 2.2: Flow chart of numerical evaluation of elastic properties [64]

of an objective function that relates experimental and numerical frequencies to determine the elastic constants of the plate. The algorithms Particle Swarm, Genetic and Pattern Search were used in the optimisation process to estimate the material elastic constants.

2.3 Algorithms for optimisation

A generic optimisation problem can be written in the following way, as presented in [66]:
Find an n-vector $\mathbf{x} = (x_1, x_2, ..., x_n)$ of design variables to minimise an objective function:

$$f(\mathbf{x}) = f(x_1, x_2, ..., x_n) \tag{2.4a}$$

subject to the p equality constraints:

$$h_j(\mathbf{x}) = h_j(x_1, x_2, ..., x_n) = 0; j = 1 \quad \text{to} \quad p \tag{2.4b}$$

and the m inequality constraints:

$$g_i(\mathbf{x}) = g_i(x_1, x_2, ..., x_n) \leq 0; i = 1 \quad \text{to} \quad m \tag{2.4c}$$

To fully define an optimisation problem it is fundamental to know what are the design variables, the objective function and any constraints that might influence the optimisation solution. One other aspect that has strong influence is the optimisation method. This thesis will be focused on Nature-inspired metaheuristic algorithms. The use of these algorithms raise some questions when the complexity and diversity of real-world problems are taken into consideration. Since most algorithms are tested against benchmark functions it is impossible to say that to solve a real-world problem algorithm A is better than algorithm B, as stated by the No-free-lunch Theorem [67]. Therefore, in this section, the algorithms selected are presented, and a more in-depth analysis is taken in order to understand how they work.

2.3.1 Description of algorithms

Nature-inspired algorithms are inspired by natural phenomena. They make use of stochastic ideas and random numbers, given an objective function, design variables and constraints. This approach is also referred to as Nature-inspired metaheuristic methods, as they start from an initial guess when solving the optimisation problem and can search very large spaces for potential solutions [66]. These algorithms were chosen because they are derivative-free, thus not requiring the calculation of analytical or numerical derivatives of the objective function. Another characteristic that makes these methods so attractive is that they can be applied to any kind of function because they only evaluate the function values. The algorithms selected to solve the proposed optimisation problem are the Genetic algorithm, the Particle Swarm Optimisation, the Grey Wolf Optimiser, the Firefly algorithm and the Cuckoo Search algorithm. These algorithms are described below.

2.3.1.1 Genetic algorithm

The Genetic algorithm (GA) is one of the most cited algorithms of all times, this algorithm was developed by Holland [15]. In essence, a genetic algorithm is a search method based on the abstraction of

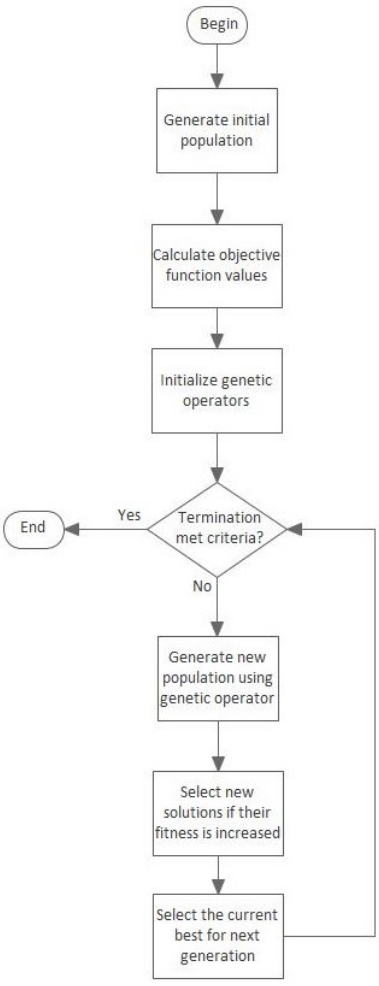

Figure 2.3: Flow Chart of Genetic algorithm

Darwinian evolution and natural selection of biological systems [10].

This algorithm is a population-based algorithm. It starts with a set of designs (population) that are randomly generated within boundaries for each design variable, as well as the fitness value. From this initial population, a random set is selected converging towards the more fit members of the set. A new generation is created using biological operators, such as crossover, mutation, and selection of the fittest. Crossover is a process that consists of swapping parts of the solutions with other solution representations. This process role is to mix the solutions and convergence in a subspace. The mutation changes a part of one solution increasing the diversity of the population, allowing to escape local minima. The last operator is the selection of the fittest. This operator uses solutions with the best fitness to pass to on to future generations.

This process of selecting the more fit solution is repeated throughout the generations (iterations) until a termination criterion is met or the maximum number of generation is met. The flowchart of this process is represented in Figure 2.3.

The source code used for this algorithm is presented in the Optimization Toolbox of MATLAB® [68].

2.3.1.2 Particle Swarm Optimisation algorithm

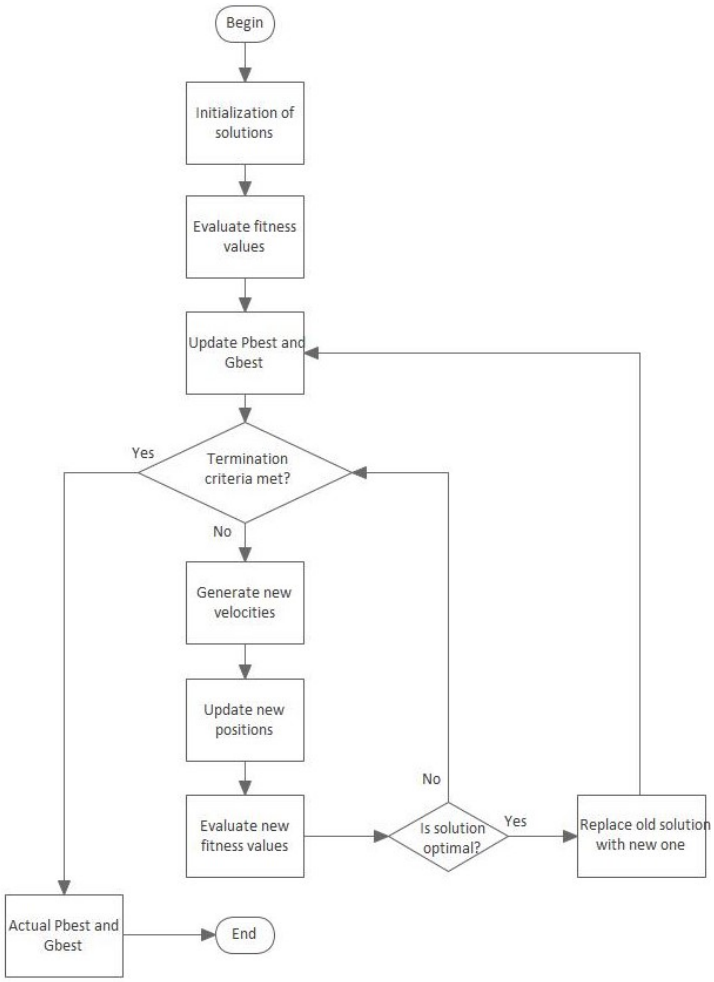

Figure 2.4: Flowchart of Particle Swarm [69]

The Particle Swarm Optimisation (PSO) algorithm takes inspiration from the group behaviour of animals, such as swarm intelligence of fishes and birds and even by human behaviour [24].

The multiple search agents, called particles, $p_1, .., p_n$, move around the search space starting from an initial random guess. The feasible solutions are called "swarm" , $P = \{p_1, ..., p_n\}$. The swarm communicates the current best and shares the global best in order to focus on the best solution found. To solve most of the problems, the number of particles used varies from twenty to fifty [67].

In Figure 2.4, it is possible to understand how the PSO works throughout the optimisation process. The particles are initialised with their position in the search space, within the boundaries defined, representing the generation zero. After determining the fitness function for this first particle values, the solution is analysed, the best solution is determined and stored. Since this is the first best, the algorithm termination is not met, and so velocity vectors are generated for each search agent. Their position is updated, and new fitness values computed. The algorithm evaluates the new fitness values and determines the new best fitness. The new best fitness is then compared to the global best, and if it is better than the global best, it replaces it. The termination criteria are then evaluated, and if the termination criteria are met, the optimisation process ends returning the optimum values. If not, the iterative process will continue until the desired termination criteria are met.

The source code used for this algorithm is presented in the Optimization Toolbox of MATLAB® [68].

2.3.1.3 Grey Wolf Optimisation algorithm

The Grey Wolf Optimisation (GWO) algorithm takes inspiration from the social hierarchy and hunting behaviours of grey wolves, as they are apex predators, meaning they are in the top of the food chain, with a strict social dominant hierarchy. This social hierarchy is well defined, and the grey wolf leaders are denominated as alphas, α, the next level in the hierarchy are the betas, β, followed by the omegas, ω, and the deltas, δ, in the bottom of the pyramid. The hunting behaviour has different stages starting with encircling prey, followed by hunting, attacking prey and search for prey [50].

Figure 2.5 describes the GWO algorithm. This algorithm starts with the grey wolf population initialisation, $\mathbf{x}_i (i = 1, 2, ..., n)$, consisting of random values for the position of each wolf. Also initialised are some algorithm-specific parameters. The fitness of each search agent is calculated, and the best search agents are selected. The termination criteria are tested, and if not met the position of the search agents are updated.

The fitness of each updated search agents is calculated. If this fitness is better than the existing best search agents (α, β and δ), then they will be replaced for the best existing solution. If it is not better than the existing best solution, the position of the current search agents is then updated. The termination criteria are tested again, and the algorithm will continue until the termination criteria are met, or the maximum number of iterations is reached.

The source code used for this algorithm is presented by Mirjalili in the MATLAB Central File Exchange [70].

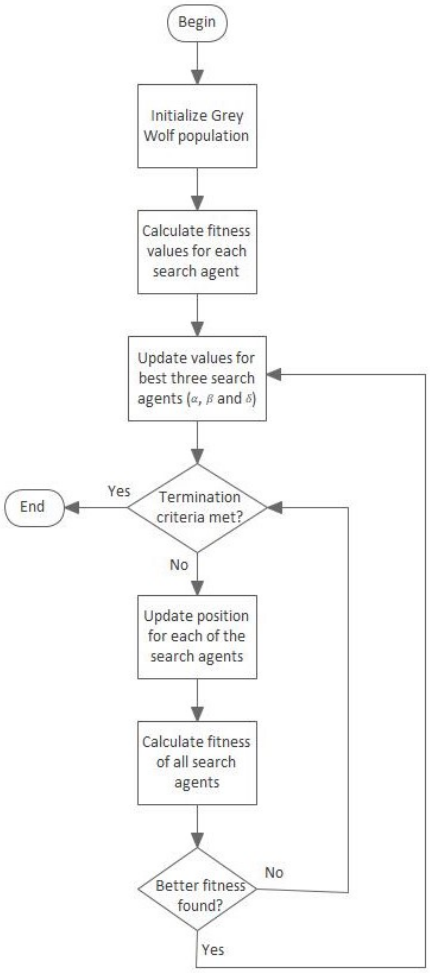

Figure 2.5: Flowchart of the Grey Wolf algorithm

2.3.1.4 Firefly algorithm

The Firefly algorithm (FA) takes inspiration from the bioluminescence flashes of fireflies. The primary function of these flashes is to attract matting partners and to attract potential prey. The pattern of flashes is specific to each one of the two thousand species of fireflies.

The FA was developed and implemented by Yang in 2009 [41]. This algorithm is based on three idealised rules: the first is that all fireflies are unisex, meaning that one firefly will be attracted to the others regardless of their sex; the second one is that the attractiveness is proportional to the brightness and these two factors reduce as the distance between fireflies increase, and the last one is that the less bright firefly will move towards the brighter ones, the fireflies randomly move towards the brightness.

In Figure 2.6, it is presented a flowchart of this algorithm. It starts with the initialisation of the firefly population and the evaluation of the fitness values, then the termination criteria are checked. If the termination criteria are not met, then relative distances between the fireflies are calculated and based on each firefly light brightness, the less bright fireflies will move towards the brightest ones. After that, the fitness value is evaluated, and if the fitness has improved, the new values will replace the old; if not, these new values will be discarded.

The best solution so far is found, and the termination criteria are rechecked. The optimisation process

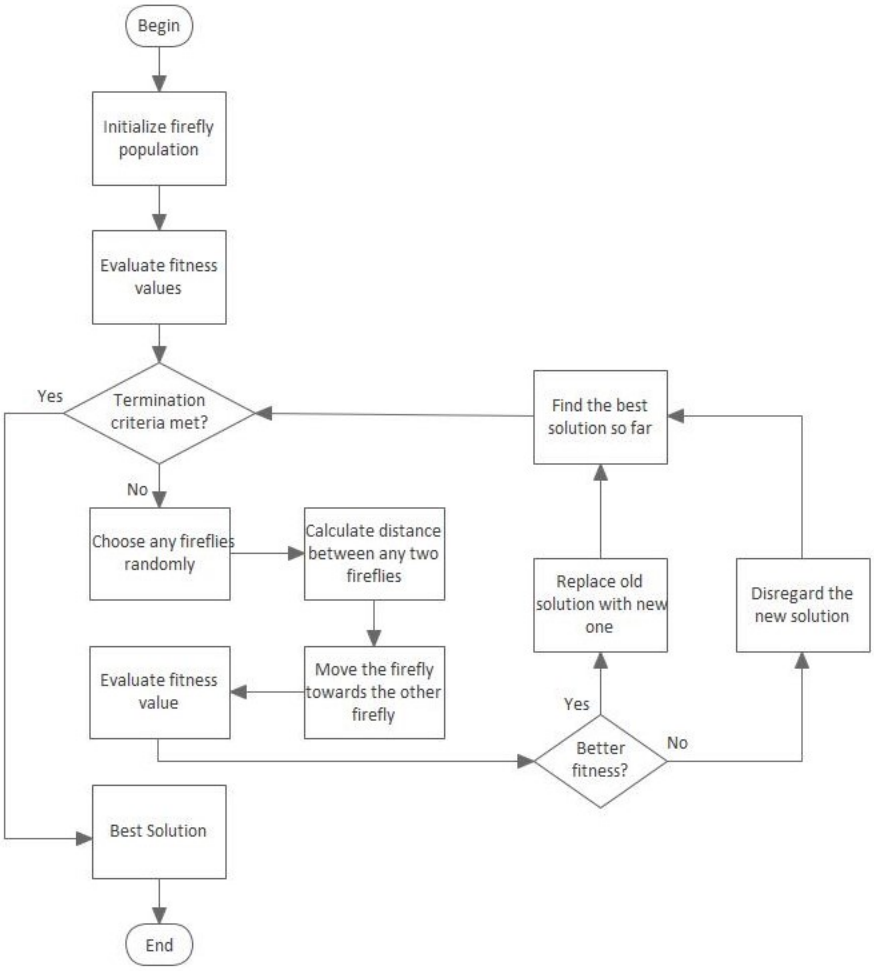

Figure 2.6: Flowchart of the Firefly algorithm [69]

will end when the termination criteria are met, and the algorithm will return as output the best solution found.

The source code used for this algorithm is presented by Yang in the MATLAB Central File Exchange [71].

2.3.1.5 Cuckoo Search algorithm

The Cuckoo Search (CS) is inspired by the brood parasitism of some cuckoo species and makes use of the Lévy flights, a behaviour of flight of many birds and insects characterised by straight flights punctuated by sudden 90° turn used to explore new terrain. This algorithm was developed by Yang and Deb in 2010 [43].

The CS can be described by three rules. The first rule is that each cuckoo lays one egg at a time in a randomly chosen nest. The second rule says that the best nest with the high-quality eggs being carried over to the next generations. The last rule is that the number of host nests is fixed, and there is a probability, $p_a \in [0, 1]$, that the host bird discovers the cuckoo's egg. In this case, the host bird can get rid of the egg or abandon the nest, creating new locations.

The flowchart in Figure 2.7 describes the CS algorithm. It starts with the initialisation of the host nest

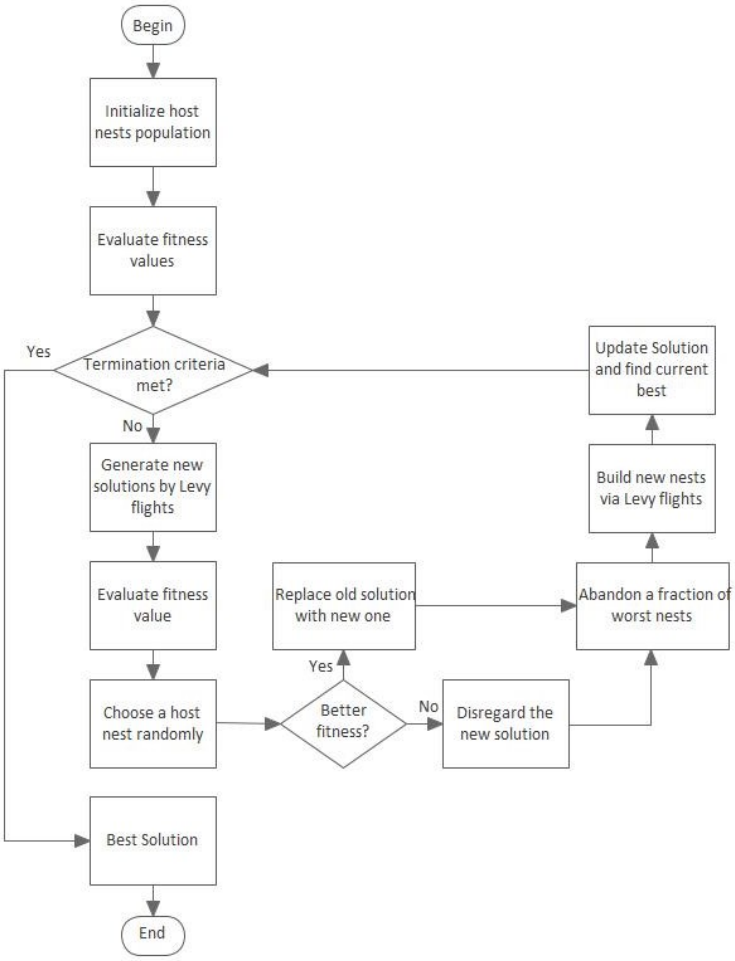

Figure 2.7: Flowchart of the Cuckoo Search algorithm [69]

population, followed by the evaluation of the fitness values. The termination criteria are checked and if not satisfied a new set of solutions are generated using Lévy flights. The fitness values are evaluated, and a random host is chosen. The new fitness value is compared with the old one, and if the new fitness value is better than the old solution, it is replaced by the new, if not, the new solution is discarded, and the old solution is kept.

After a fraction of the worst nests are abandoned, and new nests created again using Lévy flights. The solution is updated, and the current best is determined. The termination criteria are rechecked until the termination criteria are met, and the best solution is achieved terminating the algorithm.

Yang presents the source code used for this algorithm in the MATLAB Central File Exchange [72].

Chapter 3

Properties Identification

The present method for properties identification is included in the non-direct evaluation methods as it uses a metaheuristic optimisation approach for the identification of material properties. It is closely related to the work presented by Soares et al. [8], generalised by Araújo et al. [65] and further explored more recently by Lopes et al. [9].

A model of the specimen is created and natural frequencies are determined using ANSYS® Parametric Design Language (APDL). An objective function is formulated, in order to use Nature-inspired optimisation algorithms to determine the mechanical properties of specimens. This objective function relates the experimental natural frequencies ([8, 9, 65, 73, 74]) and computational natural frequencies.

3.1 Specimens selection

To apply this method, it is fundamental to measure natural frequencies using experimental techniques. In this thesis, data from previously performed measurements, taking into consideration several aspects regarding boundary conditions, material properties and specimens characteristics, will be used.

To accurately measure natural frequencies, the specimen should be suspended so that it would approximate a free condition. This condition is the one that leads to the best desired measurements. This method is applied to isotropic, transversely isotropic, orthotropic and anisotropic specimens. These specimens are rectangular plates with constant thickness. There are a large number of examples in the literature presenting data required to implement this method. However, the selected specimens were chosen as they represent some of the most used materials in composite materials, as well as some Green composites. Table 3.1 lists the selected specimens references, Table 3.2 lists the specimens materials and their geometric characteristics, and Table 3.3 lists their mechanical properties.

Table 3.1: Specimens references

Specimen	Author	Year	Reference
SP-1	Soares et al.	1993	[8]
SP-2	Lopes et al.	2019	[9]
SP-3	Araújo et al.	1996	[65]
SP-4	Larsson	1997	[73]
SP-5	Igea and Cicirello	2020	[74]

Table 3.2: Type of material and geometric characteristics of selected specimens

Specimen	Material	a x b x h (mm)	N. of Plies	Fiber Orientation
SP-1	Aluminium	193 x 281 x 1.94	1	–
SP-2	Glass-Epoxy	299.26 x 93.71 x 2.3	14	$[0^0_{14}]_T$
SP-3	Glass-Epoxy	203 x 136 x 14	-	$[0^0]$
SP-4	OSB*	2440 x 1220 x 10	-	all align
SP-5	Plywood panel	350 x 350 x 5.50	3	all align

*OSB - composite material composed of adhesive and wooden strands.

Table 3.3: Mechanical properties of selected specimens as reported in the references

Specimens	Density($\mathrm{Kg/m^3}$)	E_1(GPa)	E_2(GPa)	G_{12}(GPa)	G_{13}(GPa)	G_{23}(GPa)	ν_{12}
SP-1	2688	68.7	68.1	24.6	24.6	26.9	0.34
SP-2	1978.3	31.28	27.17	6.46	-	-	0.1659
SP-3	1886.9	42.8	12.2	4.8	4.2	4.9	0.301
SP-4	649.691	7.12	3.45	1.96	-	-	0.28
SP-5	568	8.180	4.357	0.6954	-	-	0.1216

3.2 Mesh convergence study

Since the present method relies on FEM analysis, a mesh study is carried out for all the selected specimens. Table 3.3 lists the mechanical properties extracted from references [8, 9, 65, 73, 74]. Relying on the characteristics on Table 3.2 and the mechanical properties from Table 3.3 a model for each specimen is created taking advantage of APDL®. An example of an input file is presented in Appendix A. To perform these analyses are used MATLAB® and ANSYS® to model each specimen and run the simulations required for the convergence study.

The process to obtain the requested data is as follows: MATLAB® generates an input file which contains ANSYS® script commands. In this file, the specimen plate in question is modelled and a modal analysis, also known as free vibration analysis, is requested to ANSYS®. This analysis is performed to obtain the natural frequencies and mode shapes of the plate. From the general Equation of motion, the particular case of the free vibration is deduced, assuming all applied loads and the in-plane forces are set to zero:

$$[M]\{\ddot{\Delta}\} + [K]\{\Delta\} = 0 \tag{3.1}$$

where [M] is the mass matrix, [K] is the stiffness matrix, Δ is the displacement and $\ddot{\Delta}$ is the second-order time derivative of the displacement.

In free vibration analysis the structure's behaviour is assumed to be linear, and the response can be

assumed harmonic:

$$\{\Delta\} = \{\phi_i\} cos(\omega_i t) \tag{3.2}$$

where ϕ_i is the mode shape (eigenvector) and ω_i is the natural circular frequency for mode i. By replacing this last equation in equation (3.1) yields an eigenvalue problem:

$$([K] - \omega_i^2 [M])\{\phi_i\} = 0 \tag{3.3}$$

which is solved in ANSYS® [75].

The modal analysis is requested using the APDL command **ANTYPE,MODAL**, and the arguments needed to extract the desired modal parameters. In this case are requested the number of modes, which is set using APDL argument **nmodes**. In the present work, this argument is set to ten modes. The other major option to take into account is the type of solver used, either it can be "Direct" or "Iterative". In this thesis, it is used the "Direct" or "Program Controlled" option, which results in the Block Lanczos eigenvalue extraction method with the sparse direct equation solver (**MODOPT,LAMB**)[76]. After ANSYS® finishes the calculations requested, an output file containing the final results is produced. The first ten natural frequencies are extracted from the output file.

For comparison purposes and to avoid distorted elements, the finite element dimensions were defined so that elements are approximately square. The elements used are SHELL63 (Figure 3.1) and element SHELL181 (Figure 3.2). The element SHELL63 is a four nodes quadrilateral elastic shell, and

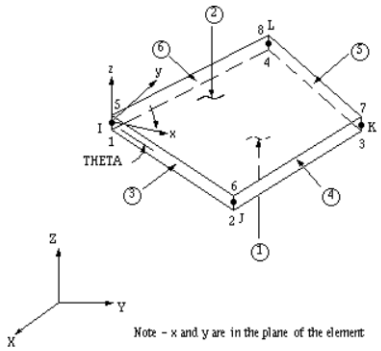

Figure 3.1: SHELL63 Geometry

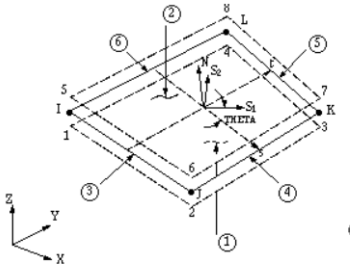

Figure 3.2: SHELL181 Geometry

so is defined by four nodes and six degrees of freedom (translations in the x, y and z directions and rotations about the nodal x, y and z axes). The element SHELL181 is a four nodes quadrilateral finite strain shell, defined by four nodes with six degrees of freedom at each node (translations in the x, y and z directions and rotations about the x, y and z axes).

For the convergence study a convergence index is used to check the mesh and help in the decision of which mesh to use for the rest of the analysis.

$$MCI = 100 \times \frac{\sum_{i=1}^{10} f_{i_{ref}} - \sum_{i=1}^{10} f_i}{\sum_{i=1}^{10} f_{i_{ref}}} \tag{3.4}$$

In Equation (3.4), the mesh convergence index (MCI) is related to the sum of the 10 natural frequencies requested, f_i, and the sum of the 10 natural frequencies of a reference mesh with approximately 10000 elements ,$f_{i_{ref}}$. In Figure 3.3, it is possible to see the convergence plots for the various specimens for SHELL63. For SHELL181 the plots can be found in Appendix B.

Analysing each case and taking into consideration the mesh convergence index, it is possible to observe that all the graphs presented in Figure 3.3 converge very quickly. The MCI is low for most of the cases, never exceeding the value of one point six per cent presented in the graph 3.3(b). All graphs converge to low values, and the highest value for the mesh convergence index for 4000 elements is obtained for graph 3.3(a). However, it is possible to see that the values have not varied more than point eight per cent. The SHELL181 convergence graphs present higher MCI than SHELL63 convergence graphs in general. The maximum MCI obtained in these graphs is around fourteen per cent converging to around one per cent.

The next tables present the selected meshes that will be used in the upcoming analysis in this thesis.

Table 3.4: Number of elements for determined Convergence Index for SHELL63 element-using 10 natural frequencies

SP-1			
MCI	# elements	a_e(mm)	a_e/a
$MCI < 0.5$%	176 (11×16)	17,55	0,09091
$MCI < 0.3$%	315 (15×21)	12,87	0.0667
SP-2			
MCI	# elements	a_e(mm)	a_e/a
$MCI < 0.5$%	252(28×9)	10.69	0.03571
$MCI < 0.3$%	1725 (75×23)	3.99	0.0133
SP-3			
MCI	# elements	a_e(mm)	a_e/a
$MCI < 0.5$%	54 (9×6)	22.56	0.1111
$MCI < 0.3$%	117 (13×9)	15.62	0.07692
SP-4			
MCI	# elements	a_e(mm)	a_e/a
$MCI < 0.02$%	392 (28×14)	87,14	0.08714
SP-5			
MCI	# elements	a_e(mm)	a_e/a
$MCI < 0.02$%	168 (14×14)	25	0.07143

In Table 3.4 are present the selected meshes that have the same MCI throughout the several spec-

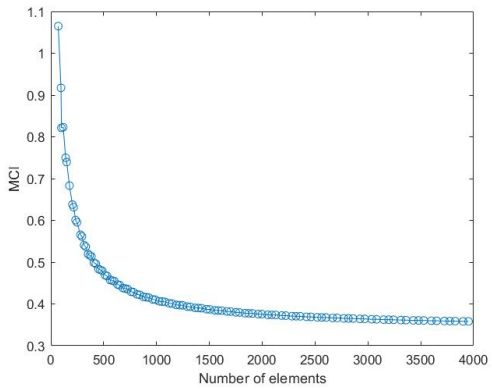

((a)) SP-1

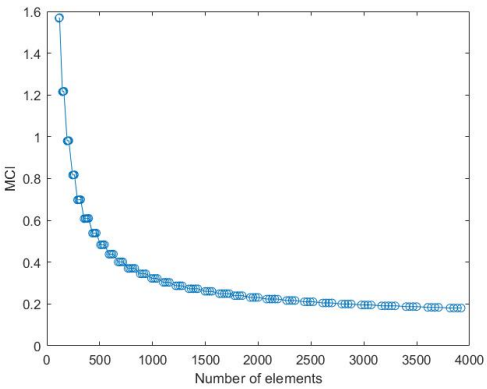

((b)) SP-2

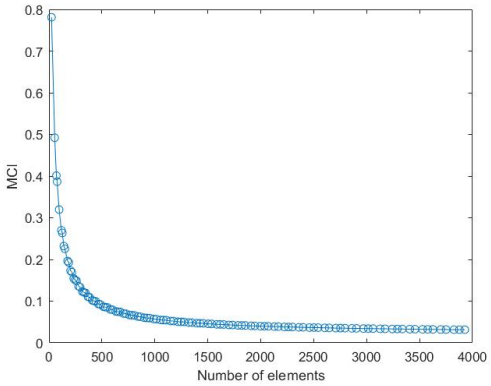

((c)) SP-3

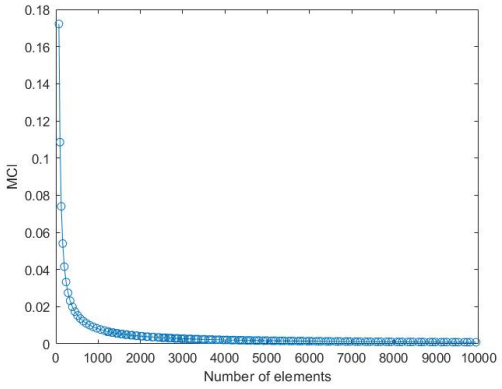

((d)) SP-4

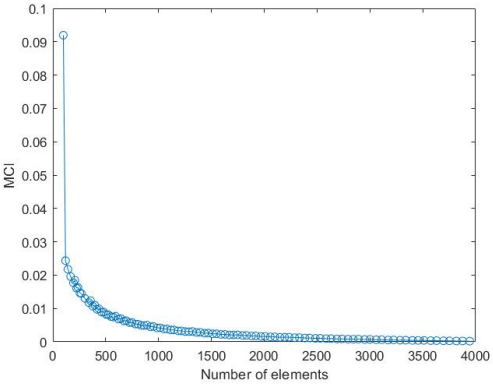

((e)) SP-5

Figure 3.3: Convergence for element type SHELL63

imens, the MCIs selected for the study using SHELL63 are $MCI < 0.5\%$, $MCI < 0.3\%$ and for some specimens $MCI < 0.02\%$ as can be seen in Table 3.4. Table 3.5 presents the meshes selected using SHELL181. The MCIs selected in this case are 0.5%, 1% and 1.5% since the graphs present higher values for the MCI.

For both of these cases, it is possible to observe that for the same MCI the adimensional dimension of the elements of each specimen stays approximately the same, or within the same order of magnitude, between all specimens . For example using SHELL63, for MCI $< 0.5\%$, SP-1 presents $a_e/a = 0.091$, SP-2 presents for $a_e/a = 0.036$ and SP-3 presents $a_e/a = 0.111$. In the next figure (Figure 3.4) are

Table 3.5: Number of elements for determined Convergence Index for SHELL181 element

SP-1			
MCI	# elements	a (mm)	a_e/a
$MCI < 1\%$	630 (21×30)	9,19	0,04762
$MCI < 0.5\%$	2772 (44×63)	4,39	0,02273
SP-3			
MCI	# elements	a_e(mm)	a_e/a
$MCI < 1.5\%$	315 (21×15)	9,67	0,04762
$MCI < 1\%$	468 (26×18)	7,82	0,03846
$MCI < 0.5\%$	950 (38×25)	5,34	0,02632

presented the mesh for this last specimens.

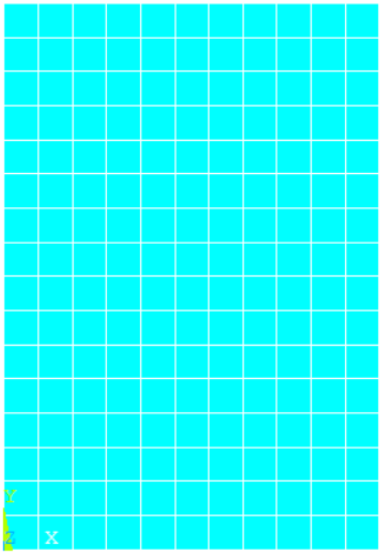

((a)) SP-1

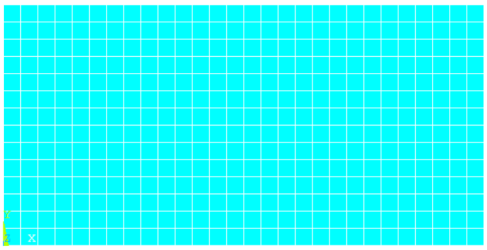

((b)) SP-4

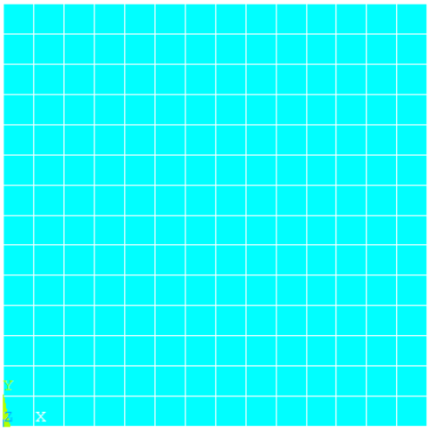

((c)) SP-5

Figure 3.4: Mesh selected using SHELL63 for SP-1, SP-4 and SP-5

After analysing the results above, the SHELL63 element graphs convergence was rapid, resulting in

the lowest MCI produced from the elements tested. Thus, meshes with MCI $< 0.5\%$ are used from now on, except for specimen SP-2. For this specimen, the mesh used presents an MCI $< 0.3\%$, corresponding to the mesh presented in the article [9] for comparison purposes.

3.3 Optimisation problems

In this section, the optimisation problems, the objective functions and the constraints applied for each specimen are presented. As seen previously in the generic optimisation problem described in section 2.3, it is necessary first to define the design variables for optimisation. In the present optimisation problems, design variables are the elastic constants of the different materials. Materials are characterised as isotropic, transversely isotropic, orthotropic or anisotropic. The Table in Figure 3.5 lists the number of elastic constants for each type of material.

Material	3D case		2D case	
	Number of non-zero constants	Number of independent constants	Number of non-zero constants	Number of independent constants
Anisotropic	36	21	9	6
Generally orthotropic	36	9	9	4
Specially orthotropic	12	9	5	4
Transversely isotropic	12	5	5	4
Isotropic	12	2	5	2

Figure 3.5: Summary of number of elastic constants for different materials [77]

In this thesis, isotropic, transversely isotropic, orthotropic and anisotropic materials are analysed. Hence, focusing on the 2D case, the number of independent elastic constants in Table 3.5 will be the same as the number of variables. The optimisation problems defined for the four different specimen material elastic constants can be represented as follows:

Isotropic materials

$$\text{Min } \Phi(E, \nu) \tag{3.5a}$$

Transversely isotropic materials

$$\text{Min } \Phi(E_1, E_2, G_{12}, \nu_{12}) \tag{3.5b}$$

Orthotropic materials

$$\text{Min } \Phi(E_1, E_2, G_{12}, \nu_{12}) \tag{3.5c}$$

Anisotropic materials

$$\text{Min } \Phi(E_1, E_2, G_{12}, G_{13}, G_{23}, \nu_{12}) \tag{3.5d}$$

The computation of the objective function is represented in the flowchart of Figure 3.6. The function inputs are the material elastic properties values that are used to perform a modal analysis in order to obtain the natural frequencies. These natural frequencies are then compared with experimental natural frequencies, through the use of an objective function.

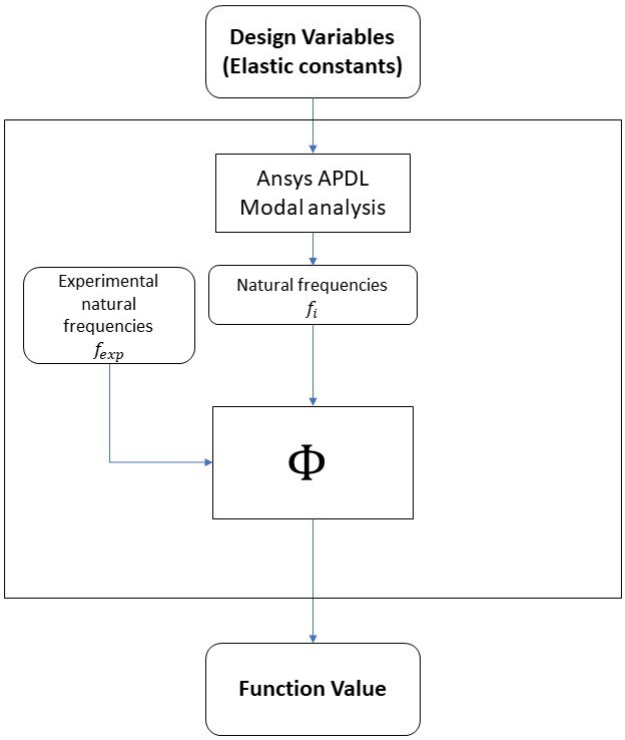

Figure 3.6: Flowchart of the objective function computation

The first objective function is presented in Equation (3.6). The objective is to minimise the sum of the absolute difference between the circular natural frequencies obtained experimentally, $\tilde{\omega_i}$, and the circular natural frequencies obtained computationally, ω_i:

$$\Phi = \sum_{i=1}^{nf} |\tilde{\omega_i} - \omega_i| \tag{3.6}$$

where nf are the total number of frequencies considered. This Equation (3.6) is defined in Lopes et al. [9]. One other objective function relates experimental circular natural frequencies, $\tilde{\omega_i}$, and computational circular natural frequencies, ω_i, according to the Equation (3.7).

$$\Phi = \sum_{i=1}^{nf} \frac{(\tilde{\omega_i}^2 - C \times \omega_i^2)^2}{\tilde{\omega_i}^4} \tag{3.7}$$

where $C = \frac{\tilde{\omega_1}^2}{\omega_1^2}$ and nf are the total number of frequencies considered for each of the specimen analysis. This objective function is presented in Soares et al. [8].

Depending on the reference article and specimen studied, the number of natural frequencies varies from five to fourteen.

The last step to have a fully defined optimisation problem is to apply the necessary constraints to the design variables. Therefore, for each specimen, a set of lower and upper constraints are defined for each one of the design variables. If the reference presents the constraints for the design variables, these are used, if not, the constraints are defined accordingly to each specific case. In Table 3.6 lists the constraints for each specimen.

Table 3.6: Constraints applied to each design variable

Specimen	Constraint	E_1(GPa)	E_2(GPa)	G_{12}(GPa)	G_{13}(GPa)	G_{23}(GPa)	ν_{12}
SP-1	Upper	100	-	-	-	-	0.4
	Lower	50	-	-	-	-	0.2
SP-2	Upper	50	50	20	-	-	0.4
	Lower	10	10	1	-	-	0.05
SP-3	Upper	70	25	15	15	15	0.4
	Lower	20	1	1	1	1	0.1
SP-4	Upper	15	10	5	-	-	0.4
	Lower	4	1	0.1	-	-	0.1
SP-5	Upper	15	10	5	-	-	0.2
	Lower	4	1	0.1	-	-	0.05

The termination criteria are the tolerance and the maximum number of iterations. The main termination criterion is tolerance. For comparison purposes, this criterion is set to 10^{-6} or 10^{-9} depending on the specimen and objective function. The tolerance is set to 10^{-6} for the other optimisation problems. This ensures that the optimisation ends when the relative difference of successive function values reaches this value. The maximum number of iterations is set to one thousand for all optimisation problems. This is needed so that, if the tolerance is not met, the algorithms will stop when they reach the one-thousandth iteration. Otherwise, the algorithm would continue indefinitely.

To solve the proposed optimisation problems needed to implement this method, the Nature-inspired metaheuristic optimisation algorithms used are the GA, the PSO, the GWO, the FA and the CS, which are described in section 2.3.1.

3.4 Optimisation problems results and analysis

3.4.1 Comparison of results obtained with different algorithms

In this section, the first set of optimisations performed are presented. These optimisations are used to verify the applicability of this method for properties identification. With this aim, the specimens SP-1 and SP-2 extracted from [8, 9] are used. For each specimen, optimisations using the five different algorithms proposed are performed. This is done so that the more suitable algorithm can be selected to be used in the next sections.

3.4.1.1 Specimen SP-1

The first optimisations are performed using specimen SP-1. The material of this specimen is isotropic. Therefore it has E and ν as design variables. It is expected to obtain values similar to the ones reported

in [8], which are listed in Table 3.3. For the presented optimisation problem, the objective function used is Equation (3.7), where nf equals nine [8]. The termination criteria are defined by a tolerance set to 10^{-9}, and the maximum number of iterations is one thousand. The design variables constraints are listed in Table 3.6. For these optimisations, the number of search agents is set to one hundred.

Table 3.7 presents the elastic constants computed, and the relative difference to the reference values [8]. All the algorithms obtain the same values for the Poisson's ratio, ν. Therefore the relative error for this design variable is the same for all algorithm. Only when analysing the values obtained for Young's modulus, E, is it possible to draw any conclusions. In this set of optimisations, this design variable presents distinct values for each of the algorithms. The best result is obtained for the PSO algorithm, presenting a relative error of zero point six per cent, followed by the GA algorithm, with a relative error of three-point four per cent. All other algorithms present relative differences above ten per cent, making them unsuitable for solving this kind of problems. These differences from the reference values are mainly due to the different method used in the optimisation process, the different finite element used to model the specimen, and the number of elements used.

Table 3.7: Elastic constants computed with each of the algorithm and relative difference for SP-1

	E (GPa)	ν	$100 * \frac{\lvert E-E_{ref}\rvert}{E}$	$100 * \frac{\lvert \nu-\nu_{ref}\rvert}{\nu}$
Reference [8]	68.7	0.34	-	-
GA	71.09	0.37	3.4	7.9
PSO	69.14	0.37	0.6	7.9
GWO	87.41	0.37	21.4	7.9
FA	78.68	0.37	12.7	7.9
CS	99.62	0.37	31.0	7.9

Table 3.8: Function values (Fval), number of iterations (Niter), number of function evaluations (NFEs) and relative computational time (RCTime) for each algorithm for SP-1

	Fval	Niter	NFEs	RCTime
GA	0.001041	65	6600	1.72
PSO	0.001041	35	3600	1.00
GWO	0.001041	996	99700	54.76
FA	0.001041	82	8200	2.65
CS	0.001041	118	11800	1.04

The function values (Fval), the number of iterations (Niter), the number of function evaluations (NFEs), and the relative computational time (RCTime) taken by each algorithm are listed in Table 3.8. The function values are equal in all algorithms. The number of iterations and the number of function evaluations have the same behaviour. The lowest number of iterations and the number of function evaluations is observed in the PSO algorithm. The lowest time is also obtained with the PSO algorithm followed by the CS algorithm, taking only a bit more than one and a half times the computation time of the PSO. However, the CS algorithm is the one that presents the highest relative difference for the design variables. The algorithm that uses more computation time is the GWO, taking more than fifty-four times the time computation of the PSO and consequently, it presents the higher number of iterations.

Figure 3.7 shows the objective function values behaviour of each of the algorithms used to solve this problem. All the algorithms tend to the same value of 0.001041. The PSO and CS algorithms are the

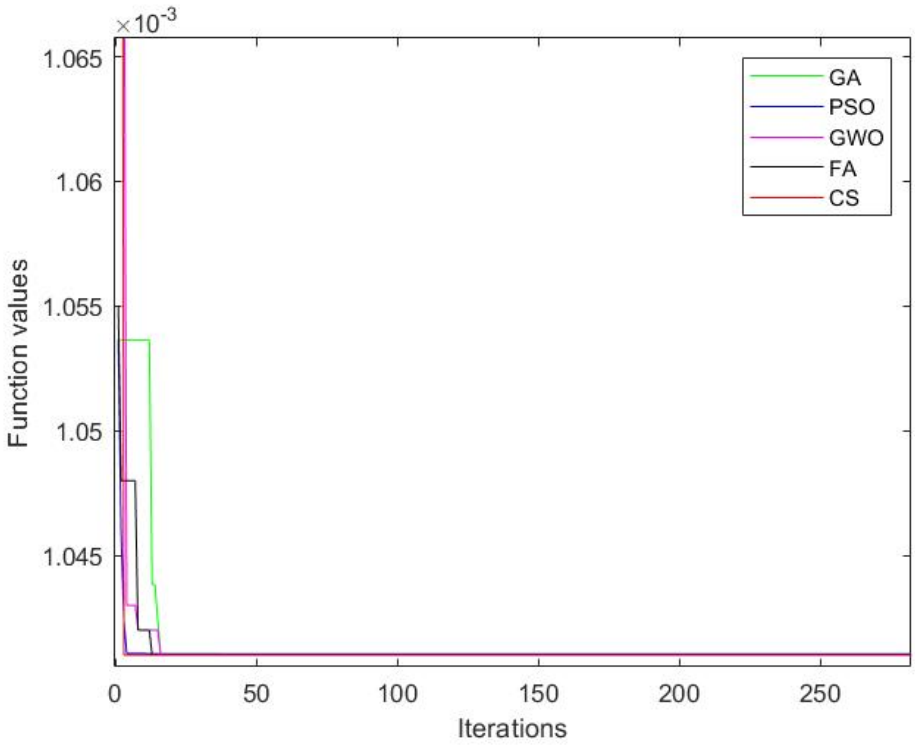

Figure 3.7: Convergence of GA, PSO, GWO, FA and CS for SP-1

fastest to reach the final function values followed closely by the FA algorithm. The PSO reached this value around the fourth iteration and the FA around the thirteenth iteration.

The dispersion of the search agents throughout the iterations for each algorithm is presented in Figure 3.8. In these graphs, the different populations of search agents created by each algorithm in the optimisation process are represented. From these graphs stands out the large number of particles presented by the GWO, 3.8(c), the FA, 3.8(d), and the CS, 3.8(e). This is not odd since these algorithms needed more iterations in order to end the optimisation process. In the GWO graph, 3.8(c), a large number of particles are present in the borders of the space, corresponding to the upper and lower bounds of the design variables, which is not desirable when solving optimisation problems.

Figure 3.8(a) presents the lowest number of particles and populations. However, most of the particles and even some populations are overlapping, not providing a good exploration of the search space. In fact, as presented in Table 3.8, the algorithm that took the lowest amount of iterations is the PSO algorithm. However, the PSO (Figure 3.8(b)) presents a good exploration of the search space with some particles in the limits of this space. Despite that, this algorithm manages to solve this problem in the lowest amount of time and iterations.

To better understand how the PSO and GWO algorithms behave throughout the iterations, four distinct populations were selected, representative of the optimisation process for each algorithm. These two algorithms correspond to the best and worst case results. The populations selected are initial population, the second population that corresponds to twenty-five per cent of the total number of iterations, the third one corresponding to fifty per cent of the iterations, and the last populations obtained. These populations are presented in Figure 3.9. The initial population in both cases has good dispersion and

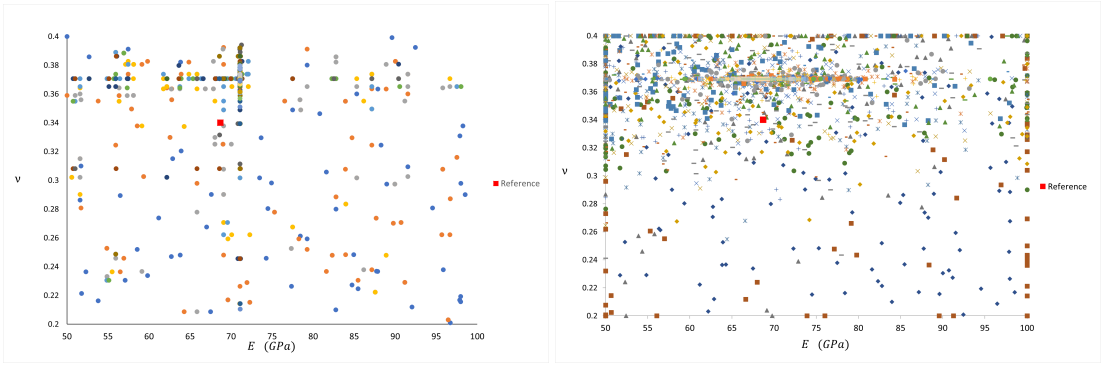

((a)) GA ((b)) PSO

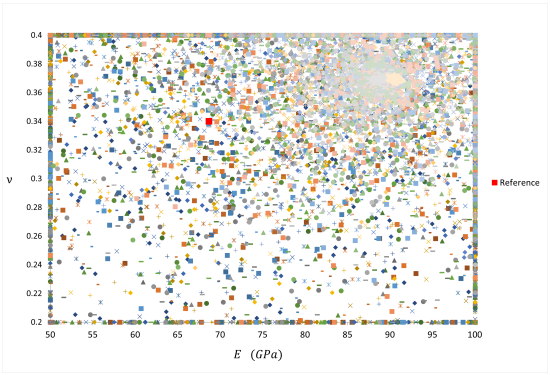

((c)) GWO

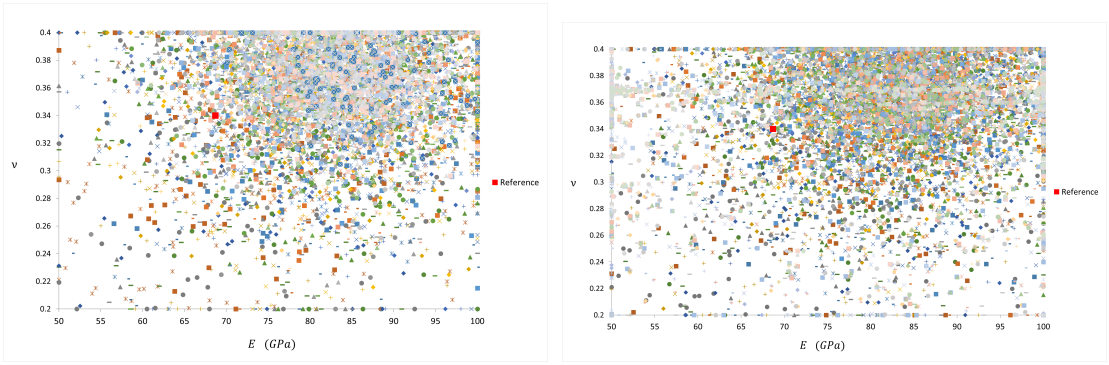

((d)) FA ((e)) CS

Figure 3.8: Dispersion of the search agents throughout the iterations for each algorithm

are scattered throughout the search space. With the increase of iterations, each algorithm is behaving differently, with the second population presented corresponding to one-quarter of the total iterations. In the PSO case, this population corresponds to the ninth iteration. At this point, the population is mostly in the upper half of the graph. The opposite can be seen for the GWO population, which is scattered through the search space and along the upper and left border of the graph. This population corresponds to the two hundred and forty-ninth iteration. At the half-point, the PSO is in the eighteenth iteration, and the GWO is in the five hundred and ninety-eighth iteration. The population of the PSO is distributed along a line in the vicinity of the reference which corresponds to the values of the elastic constants reported in the literature. The GWO population has approximately the same dispersion as before, still presenting a large number of particles in the limits of the graph. At the end of the optimisations for both cases, the populations are condensed in one small area, with the PSO population presenting a bit more

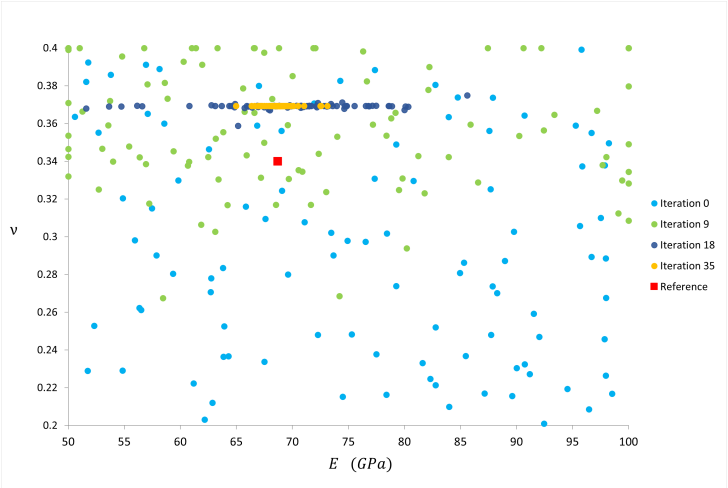

((a)) PSO

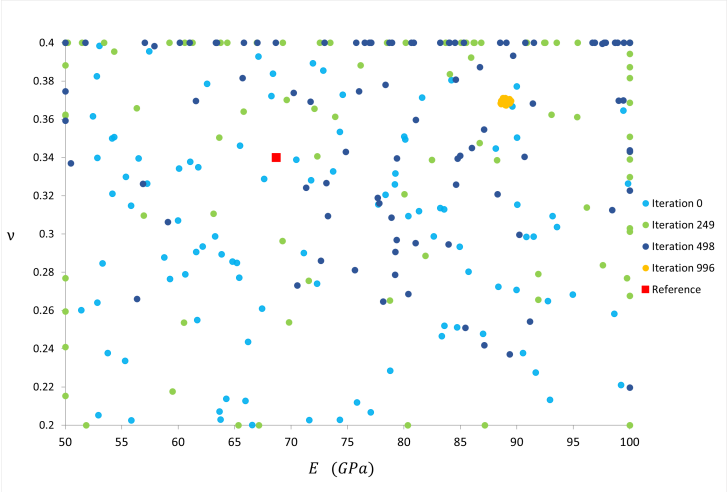

((b)) GWO

Figure 3.9: Optimisation process for the PSO and GWO algorithms: Representation of populations in the initial iteration, at 25% of the total iterations, at 50% of the total iterations and the final iteration

dispersion than the GWO population. However, the PSO population is closer to the reference value at the thirty-fifth iteration, while the GWO stops at the nine hundred and ninety-sixth iteration.

In conclusion, to solve this optimisation problem the most suitable algorithm is the PSO, which manages to obtain values for the design variables close to the reference values while using fewer iterations and time when compared to all others algorithms used.

3.4.1.2 Specimen SP-2

These second sets of optimisations are performed using the specimen SP-2. This specimen material is transversely isotropic, therefore the design variables are E_1, E_2, G_{12} and ν_{12}. The expected values are listed in Table 3.3. For this optimisation problem the objective function (Equation (3.6)), the constraints, and the search agents are the same as in reference [9]. The tolerance is set to 10^{-6}, and the number of search agents is set to one hundred. For this optimisation, nf is equal to fourteen.

Table 3.9 lists the elastic constants computed using each algorithm for this specimen. The elastic

Table 3.9: Elastic constants computed with each of the algorithms for SP-2

	E_1(GPa)	E_2(GPa)	G_{12}(GPa)	ν_{12}
Reference [9]	31.28	27.17	6.46	0.1659
GA	30.57	27.16	6.38	0.1609
PSO	30.51	27.15	6.38	0.1673
GWO	30.98	27.34	6.50	0.0885
FA	27.17	30.59	6.4	0.1579
CS	30.51	27.15	6.38	0.1676

constants computed using the different algorithms are in the vicinity of the reference values. The GWO algorithm gives the most significant variation. This last fact can be verified in Table 3.10, which presents the relative difference of the computed elastic constants with the reference values. The GWO and the FA algorithms have the greatest differences. The relative differences observed in all algorithms are due to the type of element used. Although the same number of elements is being used, the finite element used is different from the one used in reference [9]. In this article, the Kirchoff non-conforming element of four nodes and three degrees of freedom per node was used, while in this method, the shell element SHELL63 is used.

Table 3.10: Relative difference of computed elastic constants of each algorithm

	$100 * \frac{\lvert E_1 - E_{1_{ref}} \rvert}{E_1}$	$100 * \frac{\lvert E_2 - E_{2_{ref}} \rvert}{E_2}$	$100 * \frac{\lvert G_{12} - G_{12_{ref}} \rvert}{G_{12}}$	$100 * \frac{\lvert \nu_{12} - \nu_{12_{ref}} \rvert}{\nu_{12}}$
GA	2.32	0.037	1.25	3.11
PSO	2.52	0.074	1.25	0.84
GWO	0.97	0.62	0.61	87.46
FA	15.13	11.18	0.94	5.07
CS	2.52	0.074	1.25	1.01

The function values, the number of iterations, the number of function evaluations and relative time are listed in Table 3.11. The function values for most of the algorithms do not vary much. However, for the GWO algorithm, the function value obtained is around three times greater than any other. This was expected since the relative difference of this algorithm is the highest. This algorithm reaches the termination criteria of maximum numbers of iterations, reaching the one-thousandth iteration, which means that the stopping criteria of tolerance were not meet. The algorithm that took the longest was the FA, taking almost eight times more than the fastest one, the GA.

Table 3.11: Function values, number of iterations, number of function evaluations and relative computational time for each algorithm for SP-2

	Fval	Niter	NFEs	RCTime
GA	47.76	145	14600	1.00
PSO	45.66	101	10100	1.08
GWO	148.87	1000	100000	3.41
FA	48.70	916	91600	7.73
CS	45.75	622	31100	4.51

In Figure 3.10, it is possible to observe the convergence of each algorithm throughout the iterations. It is also possible to distinguish the GWO since it presents the highest function values throughout the iterations. The GA and PSO algorithms converge more quickly at almost the same rate.

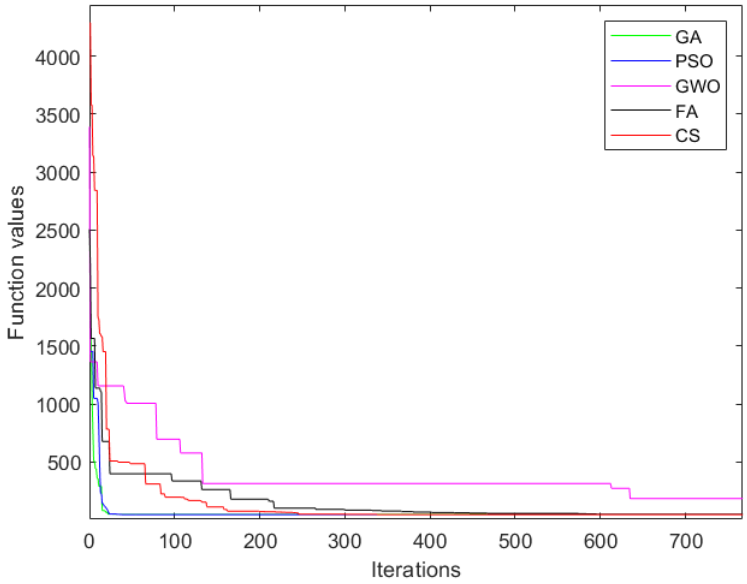

Figure 3.10: Convergence of GA, PSO, GWO, FA and CS for SP-2

All algorithms, except the GWO, tend to function values of around forty-seven. The fastest algorithm to achieve the final function value is the PSO, around the fortieth iteration.

After analysing both of these sets of optimisations, it is possible to see that the most efficient algorithms are the GA and the PSO. For both specimens, these algorithms are the ones that present the most significant results, with the lowest amount of time and iteration spent to obtain it. On the other hand are the GWO and the FA, which present the worst results while taking the largest amount of time and iterations.

3.4.1.2.1 Comparison of results with different sets of experimental natural frequencies

This specimen was presented in the article [9]. Here the authors measured experimental natural frequencies and presented a set of natural frequencies. More recently, new experimental measurements were performed in a similar plate as the one studied in [9]. In this analysis the algorithm used is the PSO algorithm for both cases. The presented method is applied to the modelled plate of this specimen, changing the input experimental frequencies for each case. Since in the more recent measurements of the natural frequencies, only ten frequencies were measured, in the present analyses, the number of frequencies used, nf, is set to ten for both cases. The set of natural frequencies presented in the article [9] is denoted as $\tilde{fi}_{a)}$ and the more recent set is denoted as $\tilde{fi}_{b)}$. For both cases the design variables constraints are kept constant, as well as the number of search agents, which are set to one hundred, and the termination criteria, with the tolerance being set to 10^{-9} and the maximum number of iterations set to one thousand. Table 3.12 lists the elastic constants computed for each case and the best function value obtained in the optimisation process.

Here it can be observed that for the Young's moduli, E_1 and E_2, the values obtained are very similar and within the acceptable values for this constant. This is also observed for the shear modulus. The

Table 3.12: Elastic constants and function value obtained for each one of the cases a) and b)

	E_1(GPa)	E_2(GPa)	G_{12}(GPa)	ν_{12}	Fval
a)	30.61	27.18	6.41	0.1555	10.21
b)	30.14	27.74	6.08	0.2000	19.15

Poisson's ratio is the elastic constant that presents the most significant variation, presenting a relative difference of around twenty per cent from the reference [9], for case b).

Table 3.13: Comparison of natural experimental frequencies and computational frequencies computed for case a) and b)

	a)			b)		
Mode	$\tilde{f}_{a)}$ (Hz)	$f_{a)}$ (Hz)	Relative difference (%)	$\tilde{f}_{b)}$ (Hz)	$f_{b)}$ (Hz)	Relative difference (%)
1	97.75	103.94	-5.9518	104.00	103.18	0.7929
2	151.75	151.71	0.0280	148.10	147.93	0.1182
3	270.25	286.98	-5.8288	285.20	285.14	0.0203
4	324.75	327.73	-0.9078	320.50	320.59	-0.0291
5	530.25	551.23	-3.8054	540.80	541.52	-0.1333
6	541.50	563.18	-3.8489	559.20	559.92	-0.1279
7	819.75	842.19	-2.6648	831.20	830.71	0.0590
8	875.75	928.27	-5.6577	922.20	922.22	-0.0025
9	1068.00	1009.31	5.8147	1026.70	1026.70	0.0004
10	1113.75	1060.42	5.0287	1076.90	1076.92	-0.0022

A modal analysis is performed next, using the elastic constants computed with both sets of experimental frequencies, and new computational natural frequencies computed corresponding to each of the sets. Table 3.13 presents the experimental frequencies used and computational frequencies computed for each of the cases. Overall, the differences between both sets of experimental frequencies are small, presenting the set b) values for the frequencies above the original set in the worst-case. The difference does not exceed fifty hertz. The biggest differences from these two measurements appear to be focused in the bending modes, such as in the first, the third, the sixth and the eighth mode. When comparing the experimental frequencies and the computational frequencies for each case, it stands out that for case a) the relative differences present greater values than in case b). In case a), the more significant differences are presented mainly in the modes corresponding to bending modes, such as the first, the third, the eighth and ninth mode. In case b), the differences between experimental and computational frequencies are drastically reduced, here the first mode presents the highest difference, presenting a value of around point eight per cent.

Figure 3.11 represents the mode shapes obtained in the modal analysis performed in ANSYS®. In this figure, the first and the eighth modes are represented: Figures 3.11(a) and 3.11(b), which are bending modes in the x direction, the ninth mode; Figure 3.11(c), which is a bending mode in the y direction, and the fourteenth mode; Figure 3.11(d), which is a mixed bending mode, with bending in the x and y direction. This last mode is obtained to compare with the ones presented in Figure 3.18. Here, this mode presents the same behaviour as in the reference [9]. However, the value of the natural frequency for this mode is closer to the one obtained in the Section 3.4.4.3 than the one presented in the reference [9].

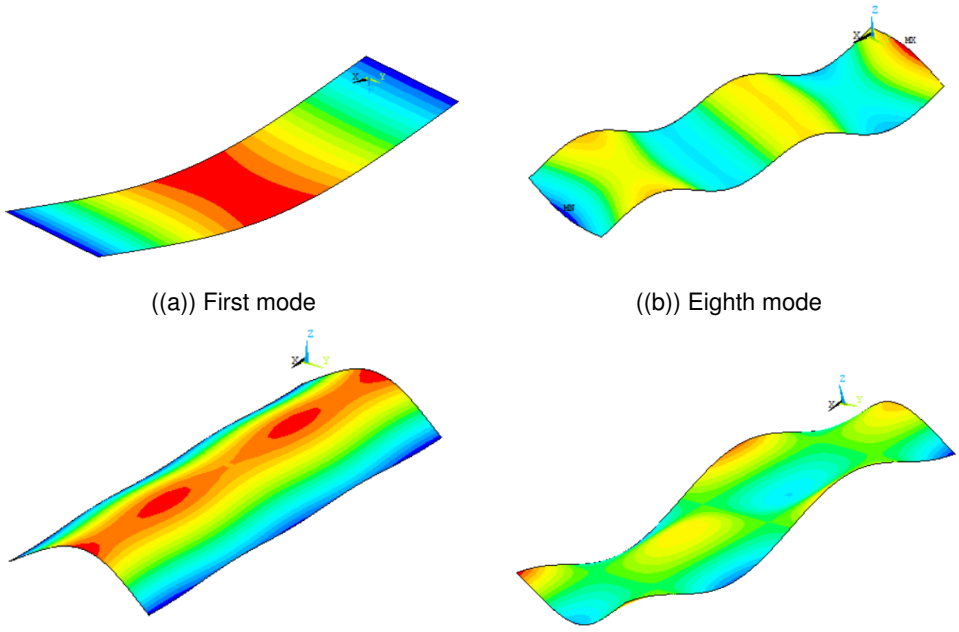

((a)) First mode

((b)) Eighth mode

((c)) Ninth mode

((d)) Fourteenth mode

Figure 3.11: Mode shape obtained using the elastic constants determined in the optimisation process using the ten natural experimental frequencies $\tilde{f}i_{b)}$

All things considered, the elastic constants computed with each set of experimental frequencies present similar values, except for the Poisson's ratio, which is proven to be more sensitive to the changes in frequency than the other elastic constants. The high sensitivity of the Poisson's ratio was also observed in [65] .

3.4.2 Comparison of results obtained with different sets of search agents

The present method is based on meta-heuristics, so there is a need to validate this method. For that, in this section, one of the most used validation tests discussed in [78] is going to be performed. This test consists of performing a specific number of runs and evaluate the values of the objective function, the design variables and the computational time. In this section, fifty optimisations are performed for SP-1 and thirty optimisations for SP-2. The objective function presented in Equation (3.6) is used for both of these optimisation problems.

The computer used in this analysis was entirely dedicated to this study while performing the optimisation process. The computer has an Intel® Core™ i7-9750H CPU @2.60 GHz processor with 16 GB of RAM. It was also used the software AMD® Radeon™ RAMDISK which allows allocating part of the computers RAM memory into a virtual disc where ANSYS® and MATLAB® can more quickly read and write the required files, thus boosting the computational performance.

3.4.2.1 SP-1

The next set of fifty optimisations are preformed for the specimen SP-1. This specimen represents the least complex problem to be solved, presenting only two design variables. For this set of optimisations,

the PSO algorithm parameters are kept constant, such as the number of search agents which is set to fifty agents per population. For the termination criteria, the tolerance is set to 10^{-6}, and the maximum number of iterations is set to one thousand iterations.

After gathering the necessary data from all the fifty optimisations, Appendix C, the averages and standard deviations of all the design variables, the objective function value and computational time are calculated and displayed in Table 3.14. The average values obtained for both elastic constants, E and ν, are close to the values showcased in the reference [8]. For the standard deviations, it presents values close to zero, with a magnitude of 10^{-14} for E, and 10^{-16} for ν which demonstrates the reliability of this method determining the material elastic constants of the material.

Table 3.14: Average and standard deviation of fifty optimisation runs for the elastic constants, function value and computational time

	E (GPa)	ν	Fval	Computational time (h)
Average	66.8	0.38	72.75	1.052
Standard deviation	0.0000	0.0000	0.0000	0.1049

The objective function values presented in all the optimisations have approximately the same value and showcasing a standard deviation with magnitude of 10^{-14}. To examine in detail the influence of each of the initial populations of search agents the computational time is studied and identified the best and worst case scenario. Figure 3.12 exhibits the computational time each optimisation process took, it is possible to see that all the optimisations took around one hour, with some peaks and dips. The optimisation which performed worst is located at a peak and the one with the best performance at a dip.

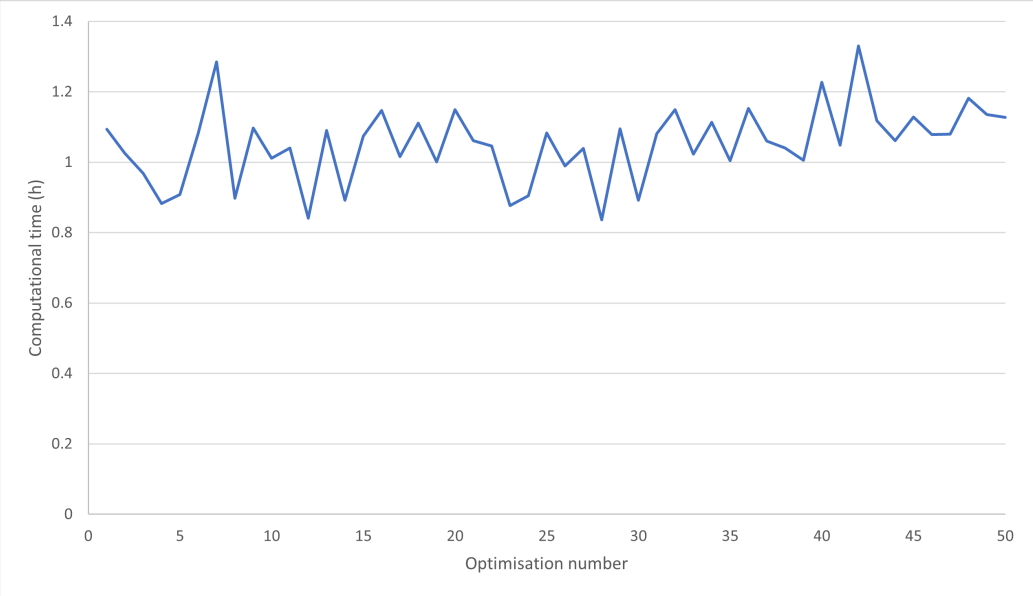

Figure 3.12: Distribution of the computational time spent by each one of the fifty optimisations with different initial population for SP-1

The best-case scenario corresponds to the twenty-eighth optimisation, which took approximately point eighty-four hours, and the worst-case scenario corresponds to the fifteenth optimisation, which took approximately one point thirty-three hours. The time difference between the best and the worst-

case is around zero point forty-nine hours, corresponding to approximately thirty minutes. The time difference between the two cases is significant, and so to understand this time difference the behaviour of the populations of the search agents are analysed for both cases. Both optimisations used different numbers of iterations, the worst-case used seventy-two iterations, and the best case used forty-six iterations. Hence, it is relevant to understand the reason for this difference. To analyse each case, the dispersions of the search agents throughout the optimisation process are represented in Figure 3.13.

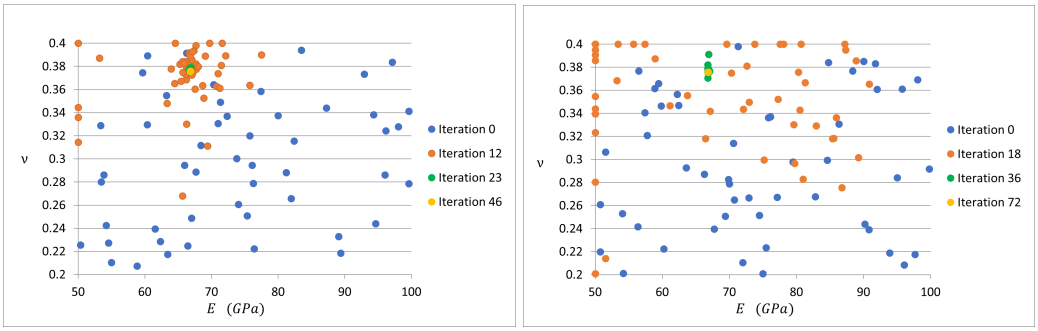

((a)) Best case ((b)) Worst case

Figure 3.13: Dispersion of the design variable throughout the optimisation process for the best and the worst case

The iterations represented in the figures correspond to the initial iteration, followed by the iteration corresponding to the one-quarter of the optimisation process, the next corresponds to half of the optimisation process and finally, the last iteration of the optimisations. For both cases, the initial population seams to explore evenly the search space, with the worst case population grouped into small swarms through the search space whereas the best case population is more scattered through the search space. The next populations represented are for the best case the population of iteration twelve which has swarmed around the final position, with some particles at the bounds. For the worst case, the population of iteration eighteen where the search agents are still scattered through the search space with a large number of agents in the bounds. At half point of both optimisations, iteration twenty-three for the best case and iteration thirty-six for the worst case, all the search agents have swarmed around the final position, which is verified by the population dispersion of the last iteration for both cases. In the best case, the optimisation termination occurred at the forty-sixth iteration, and in the worst case, the optimisation termination occurred at the seventy-second iteration. The worst case populations could not efficiently search the search space in the first quarter of the iterations. In contrast, the best case populations in the first quarter of the iterations have successfully searched the space and swarmed around the final position.

The extreme cases are computed as well making the initial population agents placed at the upper bounds and the lower bounds for the design variables. Figure 3.14 represent the dispersion of the search agents in the initial iteration, the iteration one, the one-quarter of the total number of iterations, at half of the total number of iterations and the final iterations. In these last cases, it is possible to denote that even in these extreme cases, initial populations at the constraints bounds, this method is capable of obtaining the correct elastic constants, without major variances in computational time and iterations.

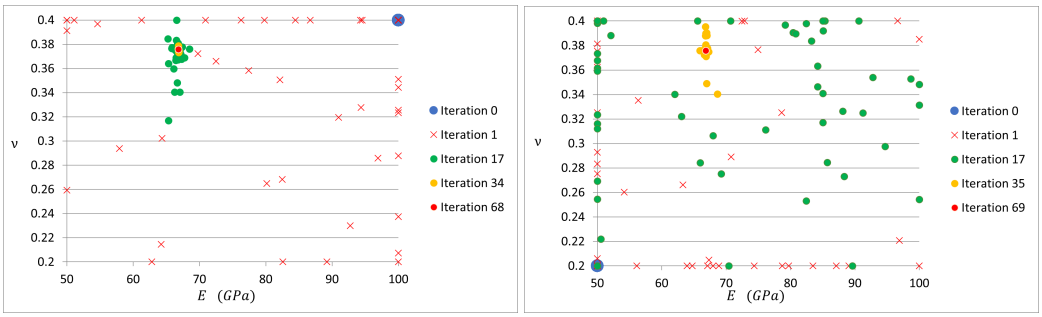

((a)) Upper bounds case ((b)) Lower bounds case

Figure 3.14: Dispersion of the design variable throughout the optimisation process for the lower bounds and the upper case

For the case of the upper bound, the termination of the optimisation process took place at the sixty-eighth iteration. The lower bounds case the termination of this optimisation occurred at the sixty-ninth iteration, both of these optimisations used fewer iterations than the worst case, Figure 3.13(b), verifying and demonstrating the independence of this method on the initial random population.

3.4.2.2 SP-2

In this section, the optimisations are performed for specimen SP-2. As described before, the problem defined with this specimen presents four design variables making it a rather complex problem to be solved.

For this analysis, the present method for properties identification is applied thirty times, and the data gathered is analysed. The algorithm parameters, such as the number of search agents, is set to one hundred for all the runs. The termination criteria are kept constant, the tolerance is set to 10^{-9}, and the maximum number of iterations is set to one thousand iterations.

The elastic constants computed in each run, as well as the objective function value and computational time, are gathered from the performed optimisation and listed in Appendix C. Table 3.15 lists the averages and standard deviations of these parameters. As it happened in the last subsection, the elastic constants average values are very close to the values produced in the specimen reference article [9] and with reduced standard deviations. In this case, the elastic constant which presents the highest variability is the shear modulus, G_{12}, with a standard deviation of 0.0067, Young's modulus E_1 showcases a standard deviation with the same order of magnitude as the shear modulus of around 0.002. The Young's modulus E_2 and the Poisson's ratio, ν_{12}, present standard deviations with the same order of magnitude smaller than for the other two design variables, for the E_2 obtaining a standard deviation of 1.53×10^{-5} and for the ν_{12} a standard deviation of 6.19×10^{-5}. The function value presents a small variation proving that despite the different initial populations, the global function minimum is determined with some certainty.

The effect of the different initial population is more noticeable in the computation time each optimisation took than in these last parameters. The computation time presents an average of around eleven hours and a standard deviation of around three point seven hours, which is significative corresponding to almost one-third of the average computational time. The computation time spent by each one

Table 3.15: Average and standard deviation of thirty optimisation runs for the elastic constants, function value and computational time for SP-2

	E_1 (GPa)	E_2 (GPa)	G_{12} (GPa)	ν_{12}	Fval	Computational time (h)
Average	30.51	27.15	6.38	0.1673	45.66	11.15
Standard deviation	0.0020	0.00001	0.0067	0.00006	0.0112	3.702

of the different optimisations is plotted in Figure 3.15. The high standard deviation of the computation time is noticeable in this figure, with the computational time varying from around six hours to as much as twenty hours. These two scenarios are the best-case scenario and the worst-case scenario, respectively corresponding to the twenty-fifth optimisation and to the twenty-first optimisation.

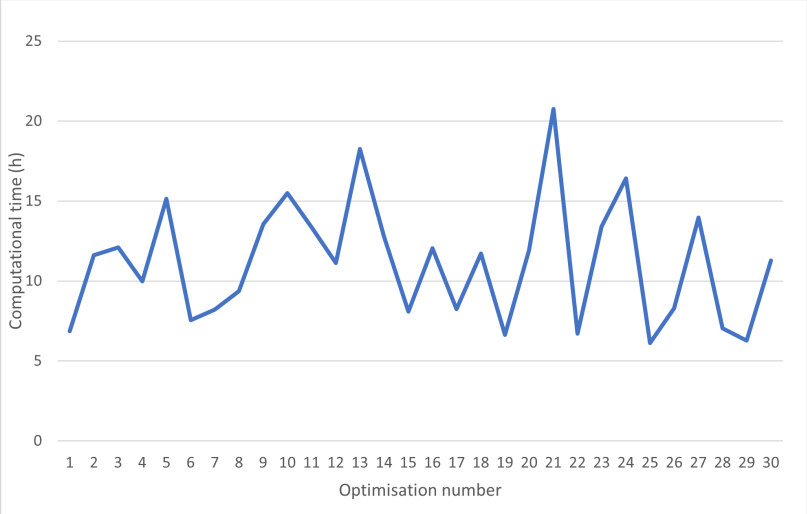

Figure 3.15: Distribution of the time spent by each one of the thirty optimisations for SP-2

In the best-case scenario, the PSO algorithm performed the optimisation process in a bit more of six hours using one hundred and thirty-four iterations. For the worst case, the PSO used more than twenty hours performing three hundred and seventy-four iteration.

In the next figure, Figure 3.16, are represented the evolution of the best values for the design variables in each iteration, side by side.

For the graphs from Figure 3.16, it is visible that the worst case scenario has a broader exploration of the search space, with its best search particles covering more scattered positions than in the best case scenario. This stands out in the v_{12} graph, Graph 3.16(h), where the search particles cover more than half of the search space before stabilising in the final value. While for the best case graphs from Figure 3.16, all the initial elastic constants are within a close range of the final value achieving this value around the fortieth iteration. Despite that, for both cases, all the design variables reached the same values when the optimisation processes ended. This is even visible in the extreme cases presented in Figure 3.17, in these cases, all the initial search agents are positioned at lower bound and upper bound of the constraints applied to the design variables. Both of these cases are extremes, all the initial search agents are positioned at the same point, and they do not randomly search all the space as all the above cases these two extremes performed better than the worst case scenario which started from a random initial population guess.

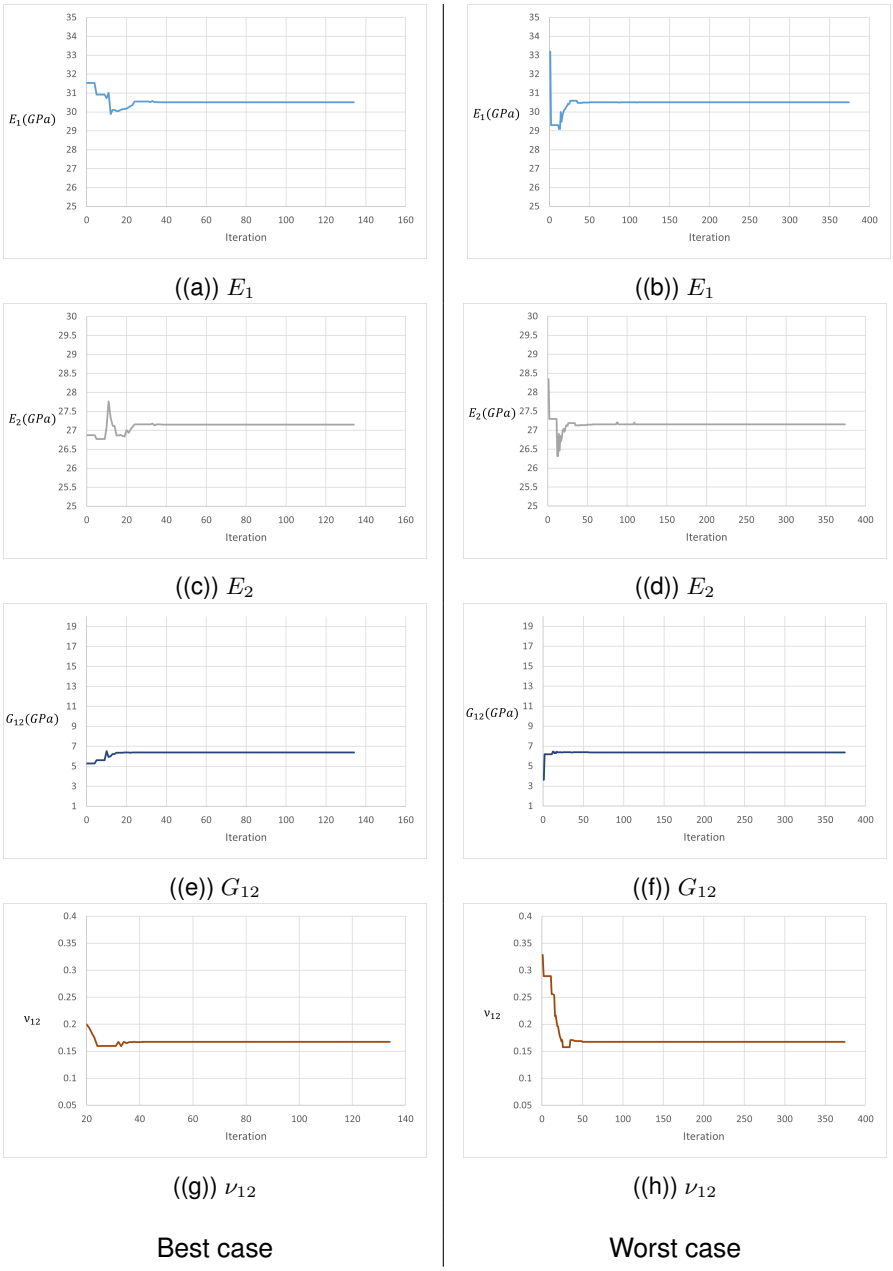

Figure 3.16: Evolution of the design variables (E_1, E_2, G_{12} and ν_{12}) values throughout iterations for both the best and worst case

These four specific optimisations, best case scenario, worst case scenario, Upper and Lower bounds cases together with the data gathered from the thirty other optimisations demonstrate that the time each optimisation uses may vary from the different set of search agent. Despite that, the validity of this method for properties identification is verified regardless of the initial set of search agents.

With the data from these two studies using SP-1 and SP-2 at least for these two kinds of optimisation problems, since each different case with different numbers of design variables represents a different optimisation problem, demonstrate the independence to achieve the correct elastic constants independently of the initial population of search agents.

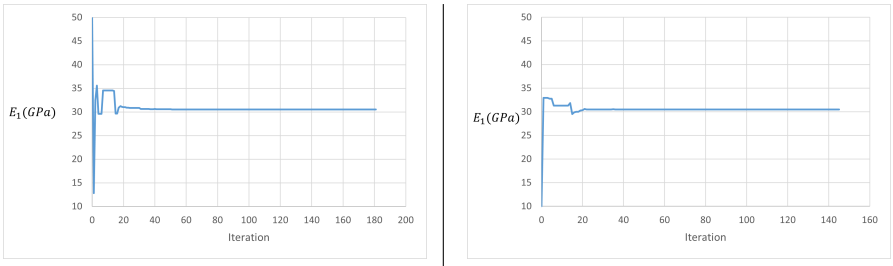

((a)) E_1 ((b)) E_1

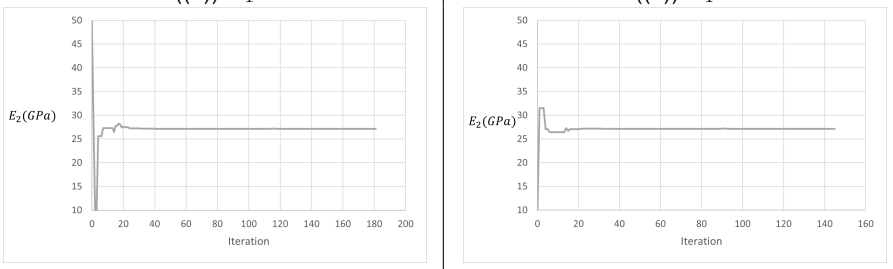

((c)) E_2 ((d)) E_2

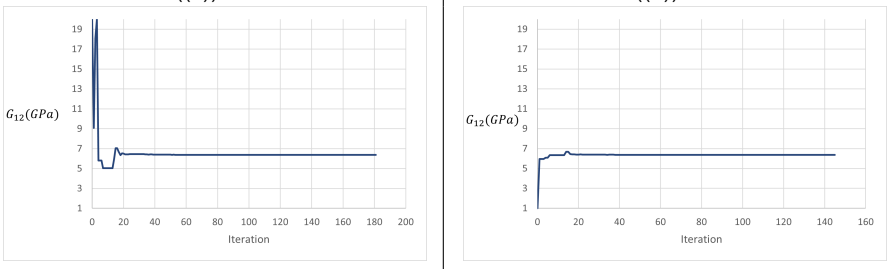

((e)) G_{12} ((f)) G_{12}

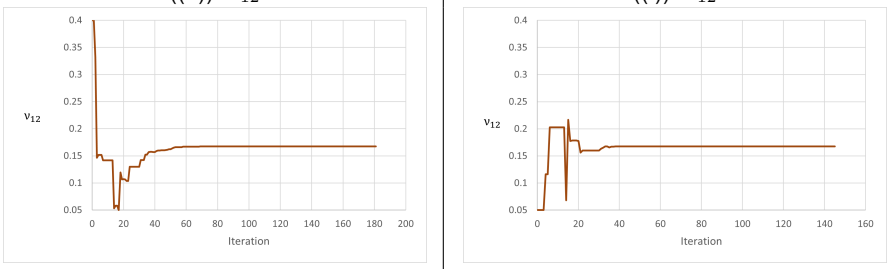

((g)) ν_{12} ((h)) ν_{12}

Upper bounds case Lower bounds case

Figure 3.17: Evolution of the design variables (E_1, E_2, G_{12} and ν_{12}) values throughout iterations for both the upper bounds case and lower bounds case

3.4.3 Comparison of results obtained with different objective functions

In this section, the objective is to study the influence of the objective function used. The optimisations are performed using the PSO algorithm, changing only the objective function. All other parameters, such as the termination criteria, are kept constant. The tolerance is set to 10^{-9} and the maximum number of iterations to one thousand. The number of search agents is set to one hundred, and the initial population is kept constant, allowing to evaluate the behaviour of the optimisation and to compare the results with the ones obtained for the same specimen with different objective functions.

In this set of optimisations the specimen used is the SP-2. The constraints for the design variables are constant. The objective functions used in this analysis are the ones used in the last section, Equation

(3.6) and (3.7) , and a new objective function:

$$\Phi = \sum_{i=1}^{nf} (fr_i - \tilde{fr_i})^2 \tag{3.8}$$

where fr_i and $\tilde{fr_i}$ are the computational and experimental frequencies, respectively, and nf the number of frequencies considered for each analysis. This objective function is presented by Tam in a review article [77].

To identify the different objective functions, in this section, the objective function in Equation (3.6) is going to be named as Φ_1, the objective function in Equation (3.7) as Φ_2 and the objective functions in Equation (3.8) as Φ_3 In the objective function Φ_1, the presence of the absolute operator serves to ensure the positivity of the objective function values. This is also achieved with the square operator seen in the objective functions Φ_2 and Φ_3. These objective functions were created in order to solve or overtake problems presented in other types of property identification methods. This is implemented either to escape second derivatives, which can be challenging to compute, for example, Φ_1, or to deal with gradient-based methods. Functions like Φ_2 and Φ_3 are known as the sum of squares and were developed to be used by gradient-based methods. Since the present method is a gradient-free method, the objective function used should have a small influence on the method. However, the functions might have a more significant influence than the expected or even just not suitable to solve the proposed kind of optimisation problem. The values obtained for the design variables, the computational time, the number of iterations each optimisation took, and the final objective function value obtained for each one of the objective functions are presented in Table 3.16.

Table 3.16: Elastic constants computed, relative computational time, number of iterations and function values obtained for SP-2 using different objective functions

Objective function	E_1(GPa)	E_2(GPa)	G_{12}(GPa)	ν_{12}	RCTime	Niter	Fval
Φ_1	30.51	27.15	6.38	0.1674	2.10	101	45.65960
Φ_2	49.99	44.48	10.53	0.1699	1.00	57	0.000068
Φ_3	30.48	27.16	6.38	0.1656	2.11	107	6.145190
Reference [9]	31.28	27.17	6.46	0.1659	-	-	-

The objective functions Φ_1 and Φ_3 obtained the best results for the computed elastic constants. The elastic constant computed with these two functions are similar and closer to the reference values than the ones obtained using Φ_2. Thus Φ_2 does not seem to be suited to solve this optimisation problem when compared to the other objective function analysed. When comparing the Φ_1 and Φ_3 values, the difference between the values obtained are minimal, and the most significant difference is in the function values.

Since Φ_1 uses slightly less time than Φ_3, thus Φ_1 is more suitable to be used to solve this type of optimisation problems.

3.4.4 Influence of the number of natural frequencies

In this section, the objective is to analyse the influence of the number of natural frequencies in the optimisation using the PSO algorithm. The algorithm parameters, such as the termination criteria, are kept constant. In the termination criteria, the tolerance is set to 10^{-6}, and the maximum number of iterations is set to one thousand.

3.4.4.1 SP-1

The specimen used in this analysis is SP-1. This specimen is presented in the article [8], where nine experimentally obtained natural frequencies are presented. For this optimisation problem, the objective function used is presented in Equation (3.6), with nf equal to nine. The number of search agents is set to fifty.

For this specimen, the design variables are Young's modulus and the Poisson's ratio. The bounds for the design variables are presented in the next Table, Table 3.17.

Table 3.17: Constraints applied to each design variable for SP-1

Specimen	Constraint	E_1(GPa)	ν_{12}
Sp-1	Upper	100	0.4
	Lower	50	0.2

The optimisation problem is now fully defined, and it is possible to solve it. In Table 3.18 the elastic constants computed using the different number of frequencies, the average, the standard deviation of the design variables, and the reference values are presented.

Table 3.18: Elastic constants computed, average and standard deviation while using PSO for each number of frequencies for SP-1

nf	E(GPa)	ν
1	68.1	0.40
2	67.9	0.39
3	67.2	0.40
4	66.7	0.38
5	67.0	0.37
6	67.5	0.34
7	66.4	0.36
8	66.4	0.36
9	66.8	0.38
Average	67.1	0.37
Standard Deviation	0.5655	0.0194
Reference [8]	68.7	0.34

The design variables have a small deviation for the different number of frequencies. The average design variables values obtained for this set of optimisations have a relative error to the reference values of around two per cent.

For this specimen, nine frequencies are used. However, with the analysis of the Table 3.18, the optimisation that came closer to the reference value of this specimen are the ones that use five frequencies.

3.4.4.2 SP-2

The next specimen used in this analysis is SP-2. In the reference article [9], fourteen natural frequencies are presented. For this optimisation problem the objective function is presented in Equation (3.6), wherein this case nf equals fourteen. The number of search agents is set to fifty, and the initial population is the same for all the optimisations.

For this set of optimisations, there are four design variables. The upper and lower bounds of the constraints for the design variables are presented in Table 3.19 and are kept constant throughout the optimisations.

Table 3.19: Constraints applied to each design variable

Specimen	Constraint	E_1(GPa)	E_2(GPa)	G_{12}(GPa)	ν_{12}
SP-2	Upper	50	50	20	0.4
	Lower	10	10	1	0.05

For these optimisations, the only variable is the different number of frequencies used in each of the optimisations. Table 3.20 lists the elastic constants computed for each number of frequencies used in the optimisation process. This Table also presents the average and the standard deviation of each one of the design variables.

The highest deviation observed for the E_1 is presented in the optimisations with four and five frequencies. The values for this design variable are approximately half of what is expected to be obtained.

Table 3.20: Elastic constants computed and its average and standard deviation, while using PSO for each number of frequencies for SP-2

nf	E_1(GPa)	E_2(GPa)	G_{12}(GPa)	ν_{12}
1	33.42	26.95	8.08	0.3422
2	33.08	27.10	6.44	0.1380
3	41.16	27.04	6.43	0.3005
4	13.48	27.03	6.46	0.1328
5	14.49	27.04	6.45	0.1388
6	25.83	27.09	6.41	0.1728
7	38.90	27.20	6.39	0.1696
8	28.82	27.11	6.40	0.1805
9	30.61	27.18	6.41	0.1550
10	30.61	27.17	6.41	0.1559
11	30.67	27.17	6.42	0.1464
12	30.60	27.15	6.41	0.1566
13	30.48	27.12	6.40	0.1705
14	30.51	27.15	6.40	0.1672
Average	29.48	27.11	6.54	0.1805
Standard Deviation	7.346	0.06847	0.4293	0.05964
Reference [9]	31.28	27.17	6.46	0.1659

The optimisation that uses fourteen frequencies presents values for the design variables very similar to the ones presented in the reference article. However, with less frequencies similar results can be obtained. The number of frequencies needed to obtain similar results is around nine frequencies.

This method uses experimentally obtained natural frequencies in order to determine the material elastic constants. In this case, these experimental natural frequencies are extracted from [9]. The

abnormal results for three, four and five frequencies, might have been the result of less accurate measurements during the experimental modal analysis. These less accurate measurements might also have been caused by the poor-quality signal captured by the laser vibrometer described in [9].

When comparing the mode shapes obtained in [9] with the ones obtained using the elastic constants obtained in the optimisation using fourteen frequencies for this plate, it is possible to observe the similarity between the three displacement modes presented. In Figure 3.18, the modes of first, ninth and fourteenth natural frequencies with displacements in the z direction are presented. For the mode shapes presented, it can be seen that the first mode, bending mode, is very sensitive to the plate elastic properties, namely in the x direction to the E_1. In contrast, the ninth mode, bending mode in the y direction, is sensitive to elastic constants E_2.

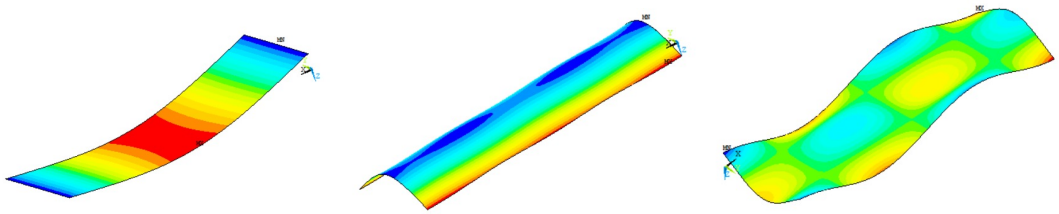

((a)) Obtained using the elastic constants obtained in the optimisation process using fourteen frequencies

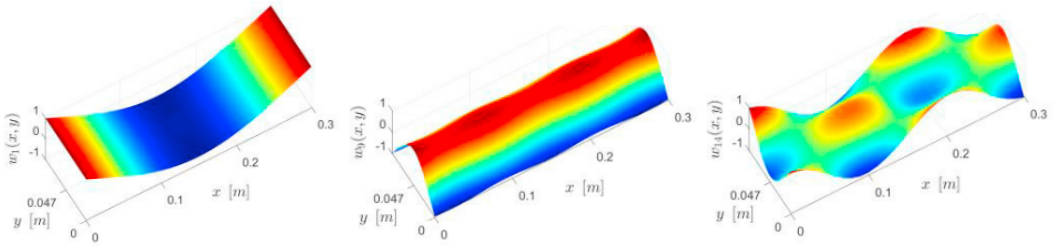

((b)) Presented in [9]

Figure 3.18: Comparison of modes of first, ninth and fourteenth natural frequencies in the z direction

When comparing both these sets of optimisations, it is possible to observe that for the SP-2, a transversely isotropic material, higher dispersion of the elastic constants is presented than for the SP-1, isotropic material. However, the complexity of each case is very different. The SP-1 only has two design variables, in comparison to the SP-2 that has four design variables, making it a much more complex problem to solve.

3.4.4.3 SP-2 with weight factor

In this subsection, a new objective function is therefore formulated based on Equation (3.6) to improve the results of this last set of optimisations and understand the influence of the number of frequencies and modes used. This new objective function is represented as the weighted difference of frequencies for each number of frequencies used.

$$\Phi = \sum_{i=1}^{nf} W_i \times |\tilde{\omega_i} - \omega_i| \tag{3.9}$$

where $\tilde{\omega_i}$ and ω_i are experimentally and computationally obtained circular frequencies, respectively. W_i is the weight factor, and nf are the total number of frequencies considered. In this case, nf equals fourteen. The optimisation algorithm used here is the PSO algorithm, and the algorithm's parameters are set to be the same as in last section 3.4.4.2. The initial population of search agents is set to fifty agents with their position being the same for each optimisation. The algorithm terminates the optimisation process when the tolerance reaches 10^{-6} or when it reaches the maximum number of iteration set to one thousand.

The weight factor in this first approach is set as zero or one, to define this factor, the experimentally determined frequencies and the computationally determined ones are compared. In this case, the computationally determined frequencies, which are obtained in the optimisation using fourteen frequencies, $nf = 14$, for the SP-2 specimen in subsection 3.4.4.2, are compared to experimental natural frequencies extracted from the article [9]. The relative difference between theses natural frequencies mode by mode is calculated, and a threshold is defined. If the threshold is met, the weight factor is set as zero, if not, it is set as one. In this case, the threshold is set to five per cent for the relative differences of frequencies. Table 3.21 lists the experimentally obtained frequencies, the computationally obtained ones, the relative differences between each frequency, and the defined weight factor.

Table 3.21: Experimentally and computationally obtained natural frequencies, relative differences calculated and weight factor defined for each mode for SP-2

Mode	$\tilde{f}$ (Hz)	f (Hz)	Relative difference (%)	W_i
1	97.75	103.78	6.17	0
2	151.75	151.60	0.10	1
3	270.25	286.62	6.06	0
4	324.75	327.55	0.86	1
5	530.25	551.02	3.92	1
6	541.50	562.56	3.89	1
7	819.75	841.99	2.71	1
8	875.75	926.96	5.85	0
9	1068.00	1010.70	5.37	0
10	1113.75	1062.30	4.62	1
11	1170.75	1193.60	1.95	1
12	1234.75	1214.10	1.67	1
13	1322.25	1399.90	5.87	0
14	1453.50	1421.70	2.19	1

The modes that present a relative difference superior to the defined threshold are the first, the third, the eighth, the ninth, and the thirteenth frequencies, and so the weight factor for these modes are set to zero. The correspondent modes shapes associated with these natural frequencies correspond to the bending modes, which are plotted in the different figures in Figure 3.19. The modes from the first, the third, the eighth and the thirteenth frequencies, Graphs 3.19(a), 3.19(b), 3.19(c) and 3.19(e), correspond to bending modes in the x direction and the mode from the ninth frequency, Graph 3.19(d), is a bending mode in the y direction.

With the weight factor set to zero these frequencies and therefore modes shapes are not considered when preforming the proposed optimisations. Therefore the maximum effective number of frequencies used in this set of optimisations is nine. Table 3.22 exhibits the effective number of frequencies used, the

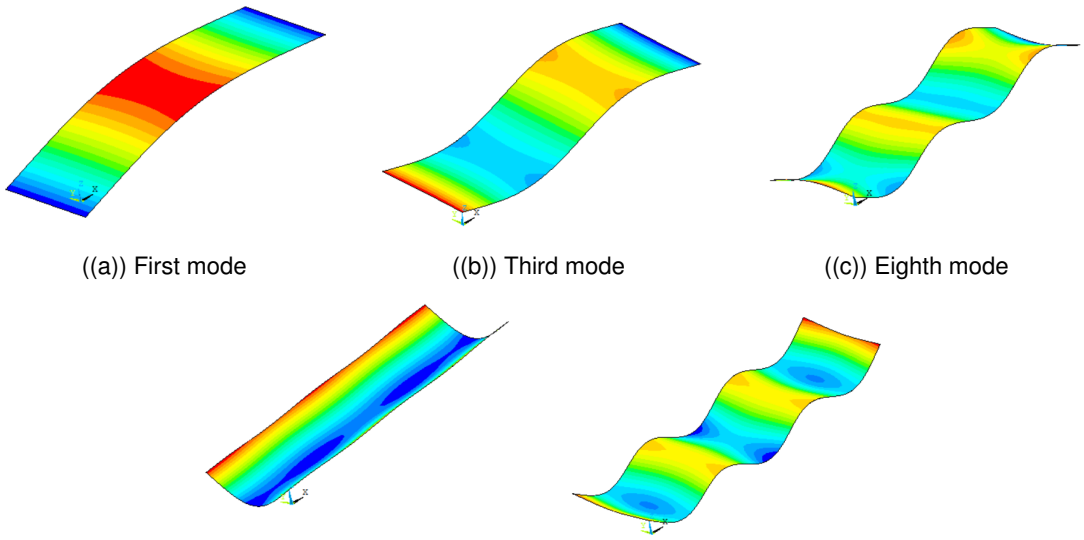

((a)) First mode ((b)) Third mode ((c)) Eighth mode

((d)) Ninth mode ((e)) Thirteenth mode

Figure 3.19: Bending modes with weight factor set to zero

elastic constants computed, and the weight factor vector considered for each case. This set of elastic constants presents an higher variation with the increase of the effective number of frequencies, for all constants when compared to the set obtained in Subsection 3.4.4.2.

Table 3.22: Effective number of frequencies considered, elastic constants computed and weight factor vector for Equation (3.9), for each number of frequencies for SP-2

Effective nf	E_1(GPa)	E_2(GPa)	G_{12}(GPa)	ν_{12}	Weight factor vector
1	14.28	46.45	6.31	0.1204	[0,1]
2	44.12	24.26	6.45	0.3551	[0,1,0,1]
3	32.57	26.62	6.35	0.3535	[0,1,0,1,1]
4	50.00	10.24	20.00	0.4000	[0,1,0,1,1,1]
5	47.71	27.25	6.38	0.1570	[0,1,0,1,1,1,1]
6	30.81	27.22	6.44	0.1304	[0,1,0,1,1,1,1,0,0,1]
7	30.29	27.05	6.44	0.1304	[0,1,0,1,1,1,1,0,0,1,1]
8	30.29	27.05	6.39	0.1888	[0,1,0,1,1,1,1,0,0,1,1,1]
9	30.69	27.20	6.42	0.1414	[0,1,0,1,1,1,1,0,0,1,1,1,0,1]
Average	34.67	28.57	7.44	0.2055	-
Standard Deviation	11.63	8.83	3.63	0.0931	-
Reference [9]	31.28	27.17	6.46	0.1659	-

Analysing this table, it is possible to observe that the for optimisation with four effective frequencies, the elastic constants obtained are equal to the upper bounds of the constraints applied to the design variables. Thus, this optimisation does not present valid results. With the increase of the number of frequencies used, the elastic constants computed get close to the values presented in the reference article [9]. With eight and nine frequencies used, the values computed for the elastic constants are similar to the reference.

In order to verify if this change in the objective function, and so experimental frequencies used, is enough to reduce the relative differences between the frequencies and therefore obtain better values for the elastic constants. The natural frequencies obtained using nine effective frequencies and the

experimental values are compared. Table 3.23 lists the new computational natural frequencies, the experimental natural frequencies and the relative difference between the two frequencies, mode by mode.

Table 3.23: Experimentally and computationally obtained natural frequencies and relative differences calculated for each mode for SP-2

Mode	$\tilde{f}$ (Hz)	f (Hz)	Relative difference (%)
1	97,75	104,06	6,46
2	151,75	151,81	0,04
3	270,25	287,22	6,28
4	324,75	327,85	0,95
5	530,25	551,27	3,96
6	541,50	563,55	4,07
7	819,75	842,04	2,72
8	875,75	929,28	6,11
9	1068,00	1007,8	5,64
10	1113,75	1058,2	4,99
11	1170,75	1190,9	1,72
12	1234,75	1213,9	1,69
13	1322,25	1399,2	5,82
14	1453,50	1416,9	2,52

When comparing these relative differences with the ones obtained in Table 3.21, it is possible to see that the same pattern observed in the first comparison is observed here as well. The modes that present the higher values for the relative difference are still the same modes presenting an increase of the relative difference in the majority of the disregarded modes.

To better understand the influence of the frequencies used and the number needed to determine the elastic constants accurately, the elastic constants computed using nf equal fourteen from Table 3.20 and the elastic constants computed for nf equals nine are compared in Table 3.24. This table lists the elastic constants computed for both cases as well the relative differences of the elastic constants to the reference article [9]. For each case is presented computational values obtained using the corresponding number of frequencies and the average values of the elastic constants computed for each one of the analysis, Tables 3.20 and 3.22.

Table 3.24: Comparison of the computed elastic constants for nf equals fourteen and for effective nf equals nine

Effective nf		E_1(GPa)	E_2(GPa)	G_{12}(GPa)	ν_{12}
-	Reference [9]	31.28	27.17	6.46	0.1659
14	Computational	30.51	27.15	6.40	0.1672
	Average	29.48	27.11	6.54	0.1805
	Computational relative difference (%)	2.462	0.07361	0.9288	0.7836
	Average relative difference (%)	5.766	0.2343	1.181	8.798
9	Computational	30.69	27.20	6.42	0.1414
	Average	34.53	27.04	6.42	0.2197
	Computational relative difference (%)	1.886	0.1104	0.6192	14.77
	Average relative difference (%)	10.84	5.135	15.10	23.85

Comparing the average values and its relative differences between both cases, it is observed that the case with nf equals nine displays greater relative differences when compared to the case with nf equals

fourteen. Despite that, the optimisation with effective nf equals nine presents better results for Young's modulus E_1 and for the shear modulus G_{12} than the optimisation which uses all fourteen frequencies. The Young's modulus E_2 obtained with fourteen frequencies displays a relative difference smaller than for the shear modulus computed in the other optimisation. For the Poisson's ratio ν_{12}, the same behaviour is displayed; however, in this case, the difference is more significant. With fourteen frequencies, the relative difference displayed is around zero point eight per cent, whereas in this case, which uses nine frequencies, the relative difference is around fifteen per cent. This behaviour the Poisson's ratio was already studied by Frederiksen which carried out a sensitivity analysis of the Poisson's ratio, according to which the sensitivity of the Poisson's ratio is very small when compared to the sensitivity of the other in-plane elastic constants [79].

With this new proposed objective function, the elastic constants computed are within the acceptable range except for the Poisson's ratio, which demonstrates being more sensitive to natural frequencies used to estimate this elastic constant.

3.4.4.4 SP-3

In this next set of optimisations, the specimen used is SP-3. This specimen is presented in the article [65], and twelve experimentally obtained natural frequencies are presented. The material of specimen SP-3 presents six independent elastic constants. This specimen represents one of the most complex problems here presented. The objective function used in this set of optimisations is presented in Equation (3.6).

For this set of optimisations, six design variables are considered. The constraints applied to each design variable are presented in Table 3.25.

Table 3.25: Constraints applied to each design variable

Specimen	Constraint	E_1(GPa)	E_2(GPa)	G_{12}(GPa)	G_{13}(GPa)	G_{23}(GPa)	ν_{12}
Sp-3	Upper	70	25	15	15	15	0.4
	Lower	20	1	1	1	1	0.1

With the optimisation problem fully defined, the optimisations can be solved. The number of frequencies used, the elastic constants computed are listed in Table 3.26. In this table, the average values, and standard deviation for each one of the design variables are also presented.

As the number of design variables increases, so does the complexity of these optimisations increases as well. The results obtained in this set of optimisations are further from the reference than in the first two sets of optimisations with fewer design variables.

In this case, analysing the average values for the design variables some discrepancies are found. Namely for the transverse shear moduli, G_{13} and G_{23}, and for the Poisson's ratio, ν_{12}. The discrepancies in the G_{13} and G_{23} are mainly because transverse shear deformations are only noticed for thick plates. As these plates are relatively thin, these moduli have low sensitivity. The discrepancies in the ν_{12} can be explained by the small sensitivity when compared to other in-plane elastic constants. This is more pronounced for anisotropic plates, which is the case of this plate [65].

Table 3.26: Computed elastic constants and its average and standard deviation while using PSO for each number of frequencies for SP-3

nf	E_1(GPa)	E_2(GPa)	G_{12}(GPa)	G_{13}(GPa)	G_{23}(GPa)	ν_{12}
1	57.8	3.6	7.9	8.6	6.4	0.275
2	39.3	19.1	4.2	7.7	9.5	0.149
3	58.6	7.8	4.3	10.0	5.9	0.159
4	49.0	9.8	3.9	3.9	1.7	0.100
5	49.7	9.4	3.7	8.6	9.1	0.244
6	49.0	9.8	3.6	6.0	11.9	0.100
7	58.7	6.4	4.0	4.1	8.9	0.157
8	44.7	8.8	4.4	1.6	4.0	0.312
9	40.7	7.9	4.7	12.6	8.9	0.251
10	35.7	15.2	2.9	9.1	11.7	0.100
11	50.6	6.0	4.6	7.9	6.3	0.225
12	49.5	6.4	4.8	5.2	10.3	0.100
Average	48.6	9.2	4.4	7.1	7.9	0.181
S. Deviation	7.2	4.0	1.2	2.9	2.9	0.074
Reference [65]	42.8	12.2	4.8	4.2	4.9	0.301

Overall, with the increased number of design variables (2, 4, 6) the complexity of each optimisation problem increases exponentially. As the number of design variables increases, the discrepancies between the results of the optimisations and the reference values increases as well. However, the major motive for the discrepancies in the computed elastic constants to the references ones are still the difference in the finite elements used and their elasticity theories.

From the number of frequencies used, a rule of thumb can be verified by the first specimen that uses two design variables and needs at least four frequencies, by the second specimen that uses four design variables needs at least eight frequencies. The last specimen, which uses six design variables needs at least twelve frequencies to obtain valid results. This means that twice as many frequencies are needed than the number of design variables.

3.4.5 Comparison of results with different number of search agents

Several optimisations are performed to study the influence of the number of search agents for the PSO algorithm, keeping constant all other parameters, including the initial position of all the search agents for all the optimisations.

The specimen used in these optimisations is the SP-2, and the objective function used is Equation (3.6), where nf equals fourteen. The constraints and the termination criteria are kept constant for all optimisations, only varying the number of search agents. The tolerance is set to 10^{-6} and the maximum number of iterations set to one thousand. In this study, the number of search agents is incremented, starting with ten agents, increasing ten agents each time until it reaches a hundred search agents.

Table 3.27 lists the elastic constants computed using the different number of search agents, the function values and the relative time for the PSO algorithm. It is possible to observe that as the number of search agents increases, the function values decrease, tending to around forty-five. For ten, twenty and forty search agents, the function values are around two thousand. The values of the Poisson's ratio, ν_{12}, for these three numbers of search agents are equal to the lower bound of the constraints applied.

Table 3.27: Elastic constants, function values and relative computational time computed for different numbers of search agents for PSO algorithm

Number of search agents	E_1(GPa)	E_2(GPa)	G_{12}(GPa)	ν_{12}	Fval	RCTime
Reference [9]	31.28	27.17	6.46	0.1659	-	-
10	37.40	10.00	20.00	0.0500	2099.55	1.00
20	37.40	10.11	20.00	0.0500	2070.54	2.75
30	30.51	27.15	6.38	0.1673	45.67	17.05
40	37.40	10.11	19.73	0.0500	2039.11	4.42
50	30.51	27.15	6.40	0.1672	45.69	11.81
60	30.51	27.15	6.40	0.1672	45.68	11.92
70	30.51	27.15	6.37	0.1674	45.65	22.24
80	30.51	27.15	6.40	0.1672	45.69	22.43
90	30.51	27.15	6.38	0.1673	45.67	17.18
100	30.51	27.15	6.38	0.1673	45.65	17.50

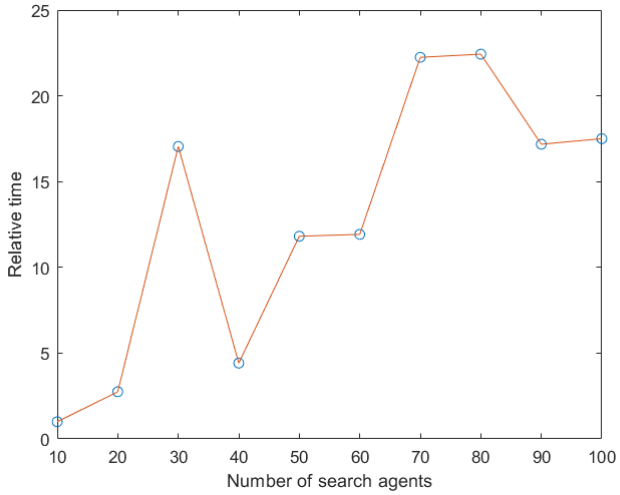

Figure 3.20: Relative time for the different number of search agents for the PSO algorithm

In the optimisation with thirty search agents, the function value has the same approximate value as the optimisation with more than fifty search agents. In Figure 3.20, it is possible to see the relative time taken by each optimisation. It presents a peak with thirty search agents and then with seventy and eighty search agents. Despite the optimisation with thirty search agents presenting good results, the time it takes is more than seventeen times the time of the optimisation with ten search agents. The optimisation with fifty search agents, when compared with the one that uses thirty, presents approximately the same results, but only uses almost twelve times the time of the optimisation with ten search agents.

To compare these results with the results presented in the article [9], the relative differences are calculated. Table 3.28 presents these relative differences of the elastic constants for each number of search agents.

As the number of search agents increases, the relative differences decrease, staying approximately constant for more than fifty agents. This is possible to observe in Figure 3.21. The largest relative differences are presented for ten, twenty, and forty search agents, in particular for E_1 and ν_{12}.

This figure presents relative differences for the design variables with the increase of search agents. The number of search agents that present the best results is thirty search agents and more than fifty

Table 3.28: Relative difference of elastic constants computed for different numbers of search agents for PSO algorithm

Number of search agents	$100 * \frac{\lvert E_1 - E_{1_{ref}} \rvert}{E_1}$	$100 * \frac{\lvert E_2 - E_{2_{ref}} \rvert}{E_2}$	$100 * \frac{\lvert G_{12} - G_{12_{ref}} \rvert}{G_{12}}$	$100 * \frac{\lvert \nu_{12} - \nu_{12_{ref}} \rvert}{\nu_{12}}$
10	212.80	27.35	67.70	231.8
20	209.50	27.35	67.70	231.8
30	15.21	10.95	1.19	0.846
40	209.49	27.35	67.26	231.8
50	15.21	10.94	0.99	0.776
60	15.21	10.94	1.04	0.793
70	15.21	10.96	1.34	0.898
80	15.21	10.94	1.01	0.787
90	15.21	10.95	1.17	0.841
100	15.21	10.95	1.25	0.868

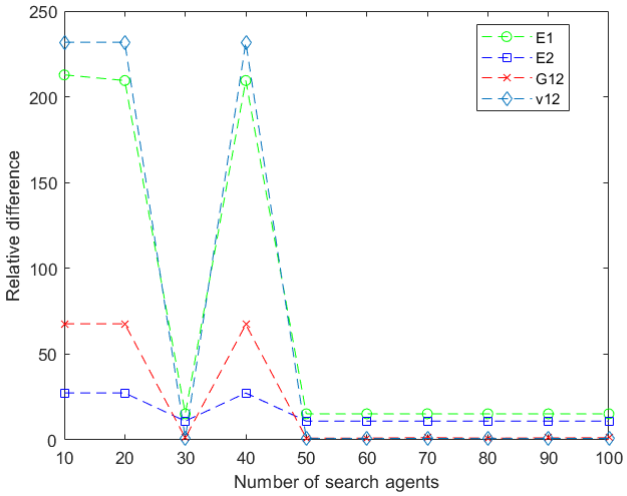

Figure 3.21: Relative difference of computed elastic constants for the different number of search agents for the PSO algorithm

search agents. These search agents present the lowest function values and the lowest relative differences.

In view of the above results, the PSO algorithm should be used with fifty search agents.

3.4.6 Green composites

In this section, the objective is to verify the applicability of this method to green composites and wood specimens. Flax fibres reinforced composites have demonstrated to be versatile in its application and with mechanical properties that could easily replace glass fibres and many others synthetic fibres. However, it was not found enough data in the literature to be able to test these flax fibres composites.

Despite that, the two specimens of green composites are studied; one of wooden strands bonded with adhesive and another of plywood of birch panels. The specimens were previously studied by Larsson and by Igea and Cicirello by using respectively a dynamic test based on modal analysis and calculated numerical eigenvalues [73]; and numerical optimisation for the estimation of elastic constants using experimental data from the Chladni patterns and experimental modal analysis [74]. These methods are introduced and their estimation of elastic constants compared to the ones computed with the present

method.

3.4.6.1 Specimen SP-4 using objective function Equation (3.6)

The specimen used in this next set of optimisations is the SP-4, which is presented in [73]. In this article, the authors proposed a method for the estimation of elastic constants based on modal analysis for a specimen of wooden strands bonded with adhesive.

This proposed method is developed for thin orthotropic rectangular plates. It is proposed that Young's moduli, E_1 and E_2, and the shear modulus, G_{12}, are estimated from the plate bending modes in the x direction, in the y direction and the first torsion mode. The Poisson's ratio is estimated from an in-plane compression mode. In this method, the author describes the in-plane free vibration problem of a plate by the coupled differential equations derived from the two-dimensional state of stress-strain equilibrium for orthotropic plates:

$$\frac{E_1}{1-\nu_{12}\nu_{21}}\frac{\partial^2 u}{\partial x^2}+\frac{E_2\nu_{21}}{1-\nu_{12}\nu_{21}}\frac{\partial^2 v}{\partial x\partial y}+G_{12}\left(\frac{\partial^2 v}{\partial x\partial y}+\frac{\partial^2 u}{\partial y^2}\right)=\rho\frac{\partial^2 u}{\partial t^2} \tag{3.10a}$$

$$\frac{E_2}{1-\nu_{12}\nu_{21}}\frac{\partial^2 v}{\partial y^2}+\frac{E_1\nu_{21}}{1-\nu_{12}\nu_{21}}\frac{\partial^2 u}{\partial x\partial y}+G_{12}\left(\frac{\partial^2 u}{\partial x\partial y}+\frac{\partial^2 v}{\partial x^2}\right)=\rho\frac{\partial^2 v}{\partial t^2} \tag{3.10b}$$

where $u = u(x, y, t)$ and $u = u(x, y, t)$ are the displacement in the x direction and the y direction respectively. The density of the material is ρ and t time. These equations can be rewritten as a function of the mode shape function, here denoted as ϕ, $u = u(x, y, t) = \phi_{C,x}(x, y)U(t)$ and $v = v(x, y, t) = \phi_{C,y}(x, y)V(t)$. From these equations, the mode shape of the first mode of compression, denoted as ϕ_C, is determined and the eigenvalue solution calculated. From the mode shape functions for the first compression mode, the value of the Poisson's ratio is estimated:

$$\nu_{12} \approx \left|\frac{\phi_{C,y}(x, y)}{\phi_{C,x}(x, y)}\right| \tag{3.11}$$

For that, the first step in this method is to preform an experimental modal analysis. In this analysis, complex frequency response functions are obtained, yielding four modal parameters such as response frequency, mode shape function, modal relative damping, and modal mass for each of the mode shapes identified. With the compression mode identified the Poisson's ratio is then estimated from mode shape values, as it is presented in Equation (3.11).

The next step is to identify the bending modes and the corresponding frequencies, so that the initial values of the elastic constants, E_1, E_2 and G_{12}, can be estimated using the next set of equations [73].

$$E_1 \approx \tilde{f_{Bx}}^2 \rho\frac{19a^4}{2\pi^2h^2} \tag{3.12a}$$

$$E_2 \approx \tilde{f_{By}}^2 \rho\frac{19b^4}{2\pi^2h^2} \tag{3.12b}$$

$$G_{12} \approx \tilde{f_T}^2 \rho\left(\frac{ab}{h}\right)^2 \tag{3.12c}$$

where $\tilde{f_{Bx}}$, $\tilde{f_{By}}$ and $\tilde{f_T}$ are the experimental frequencies corresponding to the bending in the x direction, bending in the y direction and the first torsion mode, respectively, of a plate with dimensions $a \times b \times h$. Afterwards, a finite element analysis is performed with this estimate of the elastic constant as input. The initial estimates of these elastic constants are updated as presented in the following equation for Young's modulus [73]:

$$\frac{|f_{Bx} - \tilde{f_{Bx}}|}{\tilde{f_{Bx}}} > 0.01 \Rightarrow E_1(N) = E_1(N-1)\left(\frac{\tilde{f_{Bx}}}{f_{Bx}}\right)^2 \tag{3.13}$$

where f_{Bx} is the natural frequency value computed using the finite element analysis, $\tilde{f_{Bx}}$ is the experimentally obtained natural frequency, and N the number of iterations. In order to verify that the evaluated parameters have reasonable values, the author uses Equation (3.12b), and to verify the assumed thin-plate theory uses Equation (3.12c). The last step is to determine the Poisson's ratio using the expression that originates from the Hooke's generalised law [80]:

$$\nu_{12} = \nu_{21}\frac{E_2}{E_1} \tag{3.14}$$

In the end, four estimations of the elastic constants determined are obtained. With this method, a reasonable estimate for the elastic constants of thin orthotropic plates is obtained. However, this method presents a limitation in the validation part, where the use of small-sized specimens is not representative of the average elastic properties of full-sized OSB panels [73]. Despite that, values for Young's moduli were obtained, which average, approximately ten per cent higher while using this test than using the static approach.

This specimen, SP-5, material and geometric characteristics are listed in Table 3.2. For the present study, seven natural frequencies are extracted from [73].

In this set of optimisations, the number of search agents is set to fifty. In the termination criteria, the tolerance is set to 10^{-6} and the maximum number of iteration set to one thousand iterations. Table 3.29 lists the elastic constants computed with each one of the optimisation algorithms using the objective function (3.6), and Table 3.30 lists the relative differences of each one of the computed elastic constants.

Table 3.29: Elastic constants computed with each of the algorithm for SP-4 using objective function in Eq. (3.6)

	E_1(GPa)	E_2(GPa)	G_{12}(GPa)	ν_{12}
Reference [73]	7.12	3.45	1.96	0.28
GA	7.42	2.47	2.98	0.35
PSO	7.40	2.45	2.97	0.38
GWO	7.42	2.47	2.98	0.34
FA	7.46	2.51	2.99	0.27
CS	7.39	2.44	2.97	0.40

It is possible to observe that the Young's modulus in the x direction, E_1, is the elastic constant that presents the closest values to the reference one across all algorithms, presenting a relative difference around four per cent higher than the reference value. The Young's modulus in the y direction, E_2, presents a much higher relative difference around forty per cent lower than the actual value, performing

Table 3.30: Relative difference of computed elastic constants of each algorithm using objective Function Eq. (3.6) for SP-4

	$100 * \frac{\lvert E_1 - E_{1_{ref}} \rvert}{E_1}$	$100 * \frac{\lvert E_2 - E_{2_{ref}} \rvert}{E_2}$	$100 * \frac{\lvert G_{12} - G_{12_{ref}} \rvert}{G_{12}}$	$100 * \frac{\lvert \nu_{12} - \nu_{12_{ref}} \rvert}{\nu_{12}}$
GA	4.05	39.96	34.22	19.77
PSO	3.78	40.91	34.04	26.63
GWO	4.09	39.87	34.25	18.72
FA	4.51	37.64	34.42	3.81
CS	3.63	41.47	33.95	29.88

all algorithms similarly. For the shear modulus, G_{12}, the optimisation presents values lower than the reference value, presenting across all algorithms an error around thirty-four per cent. The FA algorithms stands out when looking to Poisson's ratio, presenting a closer value to the reference among all the algorithms, presenting the lower difference only around four per cent. Table 3.31 presents the function value obtained for each algorithm. It presents the iterations and objective function count and the relative computational time spent as well for each one of the algorithms. All the algorithms reach around the same value for the function value. However, the GWO used one thousand iterations, reaching the maximum number of iterations allowed. The algorithm that took the least iterations was the PSO, needing only ninety eight iterations. Despite that, it was not the fastest one to reach the termination criteria, with the fastest being the GA algorithm. The one that took the longest time was the GWO with five hundred thousand objective function evaluations.

Table 3.31: Function value, the number of iterations, the number of function evaluations and relative computational time for each algorithm for SP-4 using objective function in Eq. (3.6)

	Fval	Niter	NFEs	RCTime
GA	120.31	111	5600	1
PSO	120.25	98	4950	1.07
GWO	120.32	1000	50000	12.94
FA	120.87	344	17200	3.65
CS	120.22	644	32200	8.97

For this specimen, this method was able to estimate the elastic constants within acceptable accuracy. However, if more frequencies were presented in the reference [73], a better estimate could be obtained. According to the thumb rule, at least twice as many frequencies are needed as the number of elastic constants, so at least eight natural frequencies would be needed. From this set of optimisations, the algorithm that had the best values computed for the design variables is the FA. Showing that depending on the optimisation problem, the most suited algorithm to be used with this method can change.

3.4.6.2 Specimen SP-5 using objective function Equation (3.6)

For this next optimisation problem, the specimen used is the SP-5. This specimen material is orthotropic, therefore the design variables are the elastic constants, E_1, E_2, G_{12}, and ν_{12}.

This specimen is presented in [74].In this article, a procedure for the evaluation of elastic constants for thin orthotropic rectangular panels is presented. The authors propose an approach that combines frequency response functions obtained via experimental modal analysis and the frequencies obtained via modal analysis to obtain the Chladni patterns. In this procedure, the operational mode shapes are

obtained with a Chladni setup. This method consists on determine four elastic constants, namely Young's moduli in the x and y directions, the in-plane shear modulus, and the Poisson's ratio. To calculate these four independent elastic constants, five natural frequencies, corresponding to the pure twisting mode, bending mode in the x and y directions, and the X and ring (O) operational mode shapes, are used. The X and ring (O) mode shapes appear due to the Poisson's ratio coupling effect [81].

The first step in this approach is to perform several experimental modal analysis and identify the resonant frequencies without evaluating the mode shapes. The next step is the Chladni setup, where the Chladni patterns are obtained. The Chladni pattern is obtained via the Chladni experimental setup where the main objective is to evaluate operational mode shapes. This experimental setup makes use of a function generator combined with an audio power amplifier connected to a loudspeaker placed on a flat horizontal surface. The test plate is positioned above the loudspeaker supported by small foam blocks which are resting in the flat surface. A fine powder, such as salt or tea leaves, is then placed on top of the plate. The speaker is used to apply a sinusoidal acoustic input and exploring a broad range of frequencies. When the driving frequency matches the panel's natural frequency, the out-of-plane vibration pattern will correspond to the operational mode shape at that frequency. As a result, the powder will move from the panel's vibrating areas to the nodal lines where no movement occurs, forming the so-called Chladni patterns showcased in Figures 3.22. These patterns are identified by the

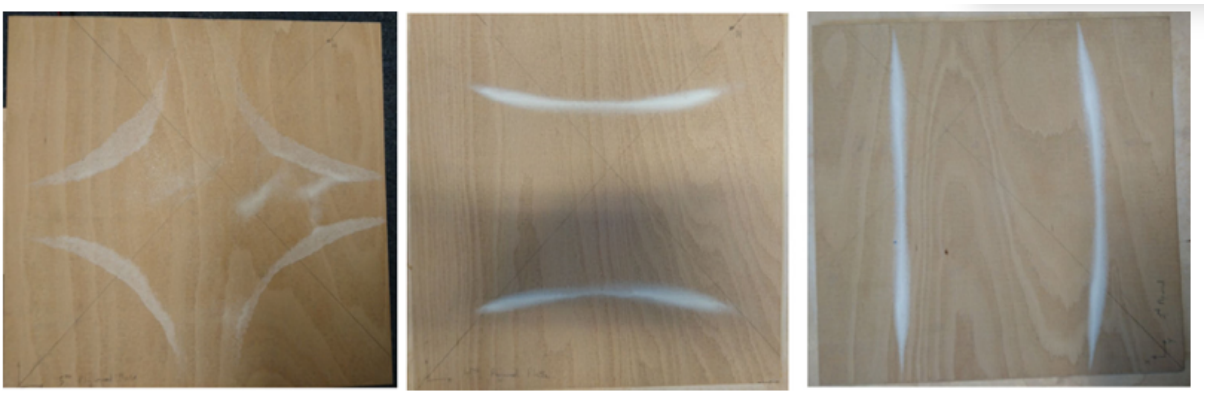

((a)) Modal shapes (+, L, H) and nodal lines obtained with the Chladni setup

((b)) Modal shapes (X, O) and nodal lines obtained with the Chladni setup

Figure 3.22: Chaldni pattern from from the proposed method [74]

shape of the powder in the plate, being identified and known the ring (O), X and cross (+) operational modal shapes. Here the frequency search is guided by the frequencies obtained in the Experimental Modal Analysis. The frequencies extracted from this method, ω, are then related with the out-of-plane harmonic response of the plate, here denoted as $\varpi(x, y)$ [81]:

$$\rho\omega^2\varpi = h^2\left[D_1\frac{\partial^4\varpi}{\partial x^4} + (D_2 + D_4)\frac{\partial^4\varpi}{\partial x^2\partial y^2} + D_3\frac{\partial^4\varpi}{\partial y^4}\right] \tag{3.15}$$

where ρ is the density, h is the thickness and the Ds are elastic constants which are related to E_1, E_2, G_{12}, ν_{12} and ν_{21} through:

$$D_1 = \frac{E_1}{12(1-\nu_{12}\nu_{21})}; D_2 = \frac{\nu_{12}E_2}{6(1-\nu_{12}\nu_{21})} = \frac{\nu_{21}E_1}{6(1-\nu_{12}\nu_{21})}; D_3 = \frac{E_2}{12(1-\nu_{12}\nu_{21})}; D_4 = \frac{G_{12}}{3}; \tag{3.16}$$

with the Poisson's ratios related by the general reciprocal theorem [82]:

$$\frac{\nu_{21}}{E_2} = \frac{\nu_{12}}{E_1}$$

From this equations the closed-form expressions are obtained and used to evaluate the constants D_1, D_3 and D_4:

$$D_4 \approx 0.274\frac{a^2b^2\rho}{h^2}\tilde{f}_+^2 \tag{3.17a}$$

$$E_1 = 0.0789\frac{12\rho a^4}{h^2}\tilde{f}_H^2 \approx 12D_1 \tag{3.17b}$$

$$E_2 = \frac{12\rho b^4}{(4.73004)^4h^2}\tilde{f}_L^2 = 0.0789\frac{12\rho b^4}{h^2}\tilde{f}_L^2 \approx 12D_3 \tag{3.17c}$$

where a, b and h are dimensions of the plate being analysed, and $\tilde{f_+}$, $\tilde{f_H}$, and $\tilde{f_L}$ are the frequencies at which the cross mode, the higher bending mode and the lower bending mode occur, respectively. In the next step the aspect ratio (a/b) is computed using Equation (3.18). The plate is cut so that the O and X operational mode shape can be displayed.

$$\frac{a}{b} = \left(\frac{D_1}{D_3}\right)^{(1/4)} \tag{3.18}$$

The Chladni test is performed again combined with the Experimental Modal Analysis and the frequencies of the O and X are recorded, and then using Equation (3.19) the constant D_2 is determined.

$$(\tilde{f}_O^2 - \tilde{f}_X^2) \approx \frac{D_2}{0.104\frac{a^2b^2\rho}{h^2}} \tag{3.19}$$

where $\tilde{f}_O$ and $\tilde{f}_X$ are the frequency of the O and X mode respectively.

The initial values of the elastic constants are used to determine the mode shapes and the natural frequencies, using the Gram-Schmidt method to construct orthogonal polynomials used as trial functions in the Rayleigh-Ritz method. The final step in this approach is to refine the values of the Ds constants as they are related directly with the elastic constants through Equations (3.16). This refinement uses an it-

erative method adjusted to minimise the difference between the predicted frequencies and the measured ones.

The present optimisation problem uses Equation 3.6, with nf equals five, to relate the experimental frequencies from [74] with the computed by this method and the constraints for the design variables as displayed in Table3.6. For this set of optimisations, the number of search agents is set to fifty. For the termination criteria, the tolerance is set to 10^{-6}, and the maximum number of iteration set to one thousand. Table 3.32 lists the computed elastic constants and Table 3.33 lists the relative differences of the elastic constants computed with the reference from [74]. The elastic constants present approximately the same values for the E_1. However, the values obtained for ν_{12}, in the PSO, the GWO, and the CS correspond to the upper bound of the constraints applied to this design variable. The largest relative differences are observed in these cases. The lowest values for the relative differences are presented for the GA algorithm, followed next for the FA algorithm.

Table 3.32: Elastic constants computed with each of the algorithm for SP-5 using objective function Eq. (3.6)

	E_1(GPa)	E_2(GPa)	G_{12}(GPa)	ν_{12}
Reference [74]	8.180	4.357	0.6954	0.1216
GA	7.388	4.507	0.7288	0.1805
PSO	7.271	4.537	0.7168	0.2000
GWO	7.256	4.537	0.717	0.2000
FA	7.896	4.399	0.736	0.0878
CS	7.271	4.537	0.7168	0.2000

Table 3.33: Relative difference of computed elastic constants of each algorithm using objective function Eq. (3.6) for SP-5

	$100 * \frac{\lvert E_1 - E_{1_{ref}} \rvert}{E_1}$	$100 * \frac{\lvert E_2 - E_{2_{ref}} \rvert}{E_2}$	$100 * \frac{\lvert G_{12} - G_{12_{ref}} \rvert}{G_{12}}$	$100 * \frac{\lvert \nu_{12} - \nu_{12_{ref}} \rvert}{\nu_{12}}$
GA	10.72	3.32	4.59	32.63
PSO	12.51	3.96	2.99	39.20
GWO	3.98	12.74	2.98	39.20
FA	0.95	3.60	5.49	38.47
CS	12.51	3.96	2.99	39.20

Table 3.34: Function values, number of iterations, number of function evaluations and relative computational time for each algorithm for SP-5 using objective function Eq. (3.6)

	Fval	Niter	NFEs	RCTime
GA	142.04	196	9850	8.37
PSO	136.20	82	4150	1.00
GWO	136.41	1000	50000	18.52
FA	176.77	1000	50000	17.87
CS	136.20	968	48400	15.90

In Table 3.34, the function values, number of iterations, number of function evaluations, and relative computational time for each of the optimisations are listed, using the different algorithms. The PSO and the CS present the lowest function value. However, these algorithms present the most significant relative difference when comparing to the reference. The GWO and the FA algorithms reach the maximum

number of iterations, thus not meeting the desired tolerance as a termination criterion. Despite that, the FA algorithm is the one that obtained better results for the E_1 and E_2.

For this specimen, the presented method did not achieve the desired results, mainly due to the low number of frequencies presented in the reference article [74]. For the presented method, at least eight natural frequencies are needed. However, the GA algorithm was able to provide some acceptable results.

Chapter 4

Conclusions

In this thesis, the main achievement was the development of a computational method for material proprieties identification in composite structures using the commercial software MATLAB® and ANSYS®. The presented method uses a derivative-free approach based on metaheuristic algorithms. This method evaluates an objective function, which relates experimental natural frequencies with computational determined natural frequencies while minimising the objective function value computed.

During this thesis were carried out several studies in which are evaluated the design variables computed for the several specimens evaluating different factors. In the first study, the objective is to select the optimisation algorithm more suited to solve the proposed optimisations problems. The algorithm that demonstrates to be more effective in obtaining the best estimative for the elastic constants is the PSO algorithm. From the tested algorithms, the PSO was the algorithm that presented best computed elastic constants while spending the least amount of computational time. It presented a relative difference of 0.6% for Young's modulus and 7.9% for the Poisson's ratio for the isotropic case. For the transversely isotropic case, SP-2, the maximum relative difference for the PSO was verified by E_2 with only 2.52%.

The next study performed was the influence of the set of experimental natural frequencies. Here, were compared the elastic constants computed with two different sets of experimental natural frequencies, verifying the high sensitivity of the Poisson's ratio, which had already been observed in [65], while obtaining good results for the other elastic constants studied. This leads to conclude that this method is moderately sensitive to the experimental frequencies. However, if the frequencies are measured within some degree of rigour and validated through multiple measurements a close estimative of elastic constants can be computed.

Since the proposed method is based on metaheuristics, the next study is a validation test. This was performed for the isotropic problem with two design variables, and the transversely isotropic problem with four design variables. Here, the method was applied multiple times for each optimisation problem with different initial populations of search agents to verify the independence of the initial position of the search agents to obtain valid values for the elastic constants which were verified for both specimens analysed. For the first specimen analysed (SP-1), was performed fifty runs of the optimisation process, the elastic constants obtained are within acceptable range with both elastic constants obtaining standard

deviations with a magnitude of 10^{-14} for the E and 10^{-16} for the ν. For the more complex case with four design variables (SP-2), was performed thirty runs of the optimisation process. In this case, the elastic constants are also within the acceptable range; the elastic constant which presented the most significant standard deviation was the shear modulus G_{12} showcasing a standard deviation of 0.0067. The data gathered from these two sets of optimisations lead to conclude that this kind of optimisation problems are independent of the initial populations generated by the algorithm to explore the search space.

The next analysis studied the influence of the number of natural frequencies used. Here, the proposed method is applied to the specimens SP-1, SP-2 and SP-3, using a different number of experimental natural frequencies to determine the material elastic constants and evaluate the differences between each case. Thus, concluding that for an accurate determination of elastic constants using this method are needed at least twice as many natural frequencies as independent elastic constants. It was also concluded that an increase of the number of experimental natural frequencies minimises the overhaul relative differences of the elastic constants with the reference. The number of search agents used in the optimisation processes is one of the parameters that influence most the efficiency of the method since more search agents explore more search space. This implies that more computational power is needed to perform more evaluations of the objective function. For this method, in the SP-2 case, the PSO algorithm should be used with fifty search agents.

One other objective of this thesis was to verify if this method for material properties identification could be applicable to green composites. This study was carried out in the last section. There, are presented two methods for the estimation of the elastic constants closely related and presented two specimens of green composites. The results obtained were close to the values presented in the references [73, 74]. However, for both cases, the number of experimental natural frequencies presented in the reference were not enough to accurately obtain the elastic constant. Nevertheless, the values obtained for the elastic constants of these specimens were in the vicinity of the values presented in the reference articles.

This method presents several advantages in comparison to other methods for material properties identification. One of the major advantages of this method is that it does not require an initial guess of the elastic constants to be computed, only requiring that the upper and lower constraints for the elastic constants are correctly defined. One other advantage is not requiring the determination of gradients to evaluate the objective function. Another advantage is that it can be easily adapted to obtain the desired elastic constants of different materials and different construction methods not requiring an extensive study of the numerical methods to estimate the material elastic constants accurately.

The most significant disadvantage is the computation time needed to generate the necessary data required so that the algorithm can evaluate the objective function and determine the function minimum, while other numerical and analytical methods require less time to estimate the elastic constants of the materials.

In a nutshell, this method has proven to be precise in computing the elastic constants of the specimens studied, as long as that enough experimental natural frequencies are provided.

The future work includes optimisation of the search algorithm used in order to reduce the computational time even more. The search for more efficient metaheuristic Nature-inspired optimisation

algorithms or any other non-derivative optimisation methods can also be considered.

For further studies, it would be interesting to have more sets of experimental natural frequencies of the same specimen to be able to, in more detail, analyse the influence of the differences in the measure of these frequencies. The analysis of more specimens with other materials and geometric characteristics using the present method is also possible. Exploring new green composites materials like the emerging flax fibres reinforced composites is also an important topic.

Bibliography

[1] C. Alves, P. Ferrão, A. Silva, L. Reis, M. Freitas, L. Rodrigues, and D. Alves. Ecodesign of automotive components making use of natural jute fiber composites. *Journal of Cleaner Production*, 18(4): 313 – 327, 2010. doi: 10.1016/j.jclepro.2009.10.022.

[2] Composites evolution launches a range of natural fibre prepregs for motorsport. https://compositesevolution.com/, Oct 2019. https://compositesevolution.com/news/composites-evolution-launches-a-range-of-natural-fibre-prepregs-for-motorsport/ (Accessed in 28/11/2020).

[3] Hybrid carbon and wood fibre car seat back. Inside Composites article, Feb 2020. https://www.insidecomposites.com/natural-fibres/hybrid-carbon-and-wood-fibre-car-seat-back/ (Accessed in 13/10/2020).

[4] Racing cars with body parts made from renewable raw materials. newsroom.porsche.com/, Sept 2020. https://newsroom.porsche.com/en/2020/motorsports/porsche-718-cayman-gt4-clubsport-mr-natural-fibre-composite-body-kit-22439.html (Accessed in 28/11/2020).

[5] J. Rodrigues and P. Martins. *Tecnologia Mecânica - Vol I*. Escolar Editora, 2010. ISBN: 978-9-72-592279-8.

[6] M. Saxena, A. Pappu, A. Sharma, R. Haque, and S. Wankhede. Composite materials from natural resources: Recent trends and future potentials. In *Advances in Composite Materials*, chapter 6. IntechOpen, Rijeka, 2011. doi: 10.5772/18264.

[7] G. Koronis, A. Silva, and M. Fontul. Green composites: A review of adequate materials for automotive applications. *Composites Part B: Engineering*, 2013. doi: 10.1016/j.compositesb.2012.07.004.

[8] C. M. M. Soares, M. M. de Freitas, A. L. Araújo, and P. Pedersen. Identification of material properties of composite plate specimens. *Composite Structures*, 17:971–978, 1993. doi: 10.1016/0263-8223(93)90174-O.

[9] H. Lopes, J. V. A. D. Santos, and A. Katunin. Identification of material properties of a laminated plate from measurements of natural frequencies and modal rotations. *Procedia Structural Integrity*, 17:971–978, 2019. doi: 10.1016/j.prostr.2019.08.129.

[10] X.-S. Yang. *Nature-Inspired Metaheuristic Algorithms Second Edition*. Number May. 2010. doi: 10.1016/j.chemosphere.2009.08.026.

[11] A. Turing and B. J. Copeland. *The essential Turing : seminal writings in computing, logic, philosophy, artificial intelligence, and artificial life, plus the secrets of Enigma*. Clarendon Press, 2004.

[12] R. Hooke and T. A. Jeeves. "Direct search" solution of numerical and statistical problems. *Journal of the Association for Computing machinery (JACM)*, 8(2):212–229, 4 1961. doi: 10.1145/321062.321069.

[13] H.-G. BEYER and H.-P. SCHWEFEL. Evolution strategies: A comprehensive introduction. *Natural Computing*, 103(3):239–248, 2002. doi: 10.1023/A:1015059928466.

[14] L. J. Fogel, A. J. Owens, and M. J. Walsh. Intelligent decision making through a simulation of evolution. *Journal of the Society for General Systems Reasearch*, 1966. doi: 10.1002/bs.3830110403.

[15] J. H. Holland. *Adaptation in Natural and Artificial Systems: An Introductory Analysis with Applications to Biology, Control and Artificial Intelligence*. 1975. ISBN: 0-262-58111-6.

[16] F. Glover. Heuristics for integer programming using surrogate constraints. *Decision Sciences*, 8(1):156–166, 1977. doi: 10.1111/j.1540-5915.1977.tb01074.x.

[17] S. Kirkpatrick, C. D. Gelatt, and M. P. Vecchi. Optimization by simulated annealing. *Science*, 220 (4598):671–680, 1983. doi: 10.1126/science.220.4598.671.

[18] F. Glover. Future paths for integer programming and links to artificial intelligence. *Computers Operations Research*, 13(5):533 – 549, 1986. doi: 10.1016/0305-0548(86)90048-1. Applications of Integer Programming.

[19] The immune system, adaptation, and machine learning. *Physica D: Nonlinear Phenomena*, 22(1):187 – 204, 1986. doi: 10.1016/0167-2789(86)90240-X. Proceedings of the Fifth Annual International Conference.

[20] J. M. Bishop. Stochastic searching networks. In *1989 First IEE International Conference on Artificial Neural Networks, (Conf. Publ. No. 313)*, pages 329–331, 1989.

[21] P. Moscato. On evolution, search, optimization, genetic algorithms and martial arts towards memetic algorithms. pages 158–79, 1989. doi: 10.1126/science.220.4598.671.

[22] A. Colorni, M. Dorigo, V. Maniezzo, F. J. Varela, and P. Bourgine. Distributed optimization by ant colonies. 1992.

[23] G. Dueck. New optimization heuristics: The great deluge algorithm and the record-to-record travel. *Journal of Computational Physics*, 104(1):86–92, 1993.

[24] R. Eberhart and J. Kennedy. A New Optimizer Using Particle Swarm Theory. pages 39–43, 1995.

[25] R. Storn. Differential Evolution – A simple and efficient heuristic for global optimization over continuous spaces. pages 341–359, 1997.

[26] H. Murase and A. Wadano. Photosynthetic algorithm for machine learning and TSP. pages 19–24, 1998. doi: 10.1016/S1474-6670(17)36035-4.

[27] M. A. Lones. Mitigating Metaphors : A comprehensible guide to recent nature-inspired algorithms. *SN Computer Science*, pages 1–12, 2020. doi: 10.1007/s42979-019-0050-8.

[28] Z. W. Geem, J. H. Kim, and G. V. Loganathan. A new heuristic optimization algorithm: Harmony Search. *SIMULATION*, (76(2)):60–68, 2001. doi: 10.1177/003754970107600201.

[29] H. A. Abbass. Mbo: Marriage in honey bees optimization: A haplometrosis polygynous swarming approach. 2001.

[30] K. M. Passino. Biomimicry of Bacterial Foraging for Distributed Optimization and Control. *IEEE Control Systems*, 22(3):52–67, 2002. doi: 10.1109/MCS.2002.1004010.

[31] M. M. Eusuff and K. E. Lansey. Optimization of water distribution network design using the shuffled frog leaping algorithm. *Journal of Water Resources Planning and Management*, 129(3):210–225, 2003. doi: 10.1061/(ASCE)0733-9496(2003)129:3(210).

[32] T. Ray and K. M. Liew. Society and civilization: An optimization algorithm based on the simulation of social behavior. *IEEE Transactions on Evolutionary Computation*, 7(4):386–396, 2003.

[33] D. Karaboga. An idea based on honey bee swarm for numerical optimization. technical report-tr06. 2005.

[34] K. Kaipa and D. Ghose. Detection of multiple source locations using a glowworm metaphor with applications to collective robotics[c]. pages 84 – 91, 07 2005. doi: 10.1109/SIS.2005.1501606.

[35] O. K. Erol and I. Eksin. A new optimization method: Big bang-big crunch. *Adv. Eng. Softw.*, 37: 106–111, 2006.

[36] S.-C. Chu, P.-W. Tsai, and J.-S. Pan. Cat swarm optimization. pages 854–858, 01 2006. doi: 10.1007/11801603_94.

[37] A. Mehrabian and C. Lucas. A novel numerical optimization algorithm inspired from weed colonization. *Ecological Informatics*, 1:355–366, 12 2006. doi: 10.1016/j.ecoinf.2006.07.003.

[38] E. Atashpaz-Gargari and C. Lucas. Imperialist competitive algorithm: An algorithm for optimization inspired by imperialistic competition. *2007 IEEE Congress on Evolutionary Computation*, pages 4661–4667, 2007.

[39] D. Simon. Biogeography-based optimization. *IEEE Transactions on Evolutionary Computation*, 12 (6):702–713, 2008. doi: 10.1109/TEVC.2008.919004.

[40] S. He, Q. Wu, and J. Saunders. Group search optimizer: An optimization algorithm inspired by animal searching behavior. *Evolutionary Computation, IEEE Transactions on*, 13:973 – 990, 11 2009. doi: 10.1109/TEVC.2009.2011992.

[41] X.-S. Yang. Firefly algorithms for multimodal optimization. In *Proceedings of the 5th International Conference on Stochastic Algorithms: Foundations and Applications*, SAGA'09, page 169–178, Berlin, Heidelberg, 2009. Springer-Verlag.

[42] H. Shah-Hosseini. The intelligent water drops algorithm: A nature-inspired swarm-based optimization algorithm. *Int. J. Bio-Inspired Comput.*, 1(1/2):71–79, Jan. 2009. doi: 10.1504/IJBIC.2009.022775.

[43] X.-S. Yang and S. Deb. Cuckoo search via levey flights. pages 210 – 214, 01 2010. doi: 10.1109/NABIC.2009.5393690.

[44] Y. Tan and Y. Zhu. Fireworks algorithm for optimization. In *Proceedings of the First International Conference on Advances in Swarm Intelligence - Volume Part I*, ICSI'10, page 355–364, Berlin, Heidelberg, 2010. Springer-Verlag. ISBN 3642134947. doi: 10.1007/978-3-642-13495-1_44.

[45] R. V. Rao, V. J. Savsani, and D. P. Vakharia. Teaching-learning-based optimization: A novel method for constrained mechanical design optimization problems. *Comput. Aided Des.*, 43(3):303–315, Mar. 2011. doi: 10.1016/j.cad.2010.12.015.

[46] X. Yang and A. H. Gandomi. Bat algorithm: a novel approach for global engineering optimization. *Engineering Computations*, 29(5):464–483, Jul 2012. doi: 10.1108/02644401211235834.

[47] X.-S. Yang. Flower pollination algorithm for global optimization. *Lecture Notes in Computer Science*, page 240–249, 2012. doi: 10.1007/978-3-642-32894-7_27.

[48] W.-T. Pan. A new fruit fly optimization algorithm: Taking the financial distress model as an example. *Knowledge-Based Systems*, 26:69 – 74, 2012. doi: 10.1016/j.knosys.2011.07.001.

[49] A. H. Gandomi and A. H. Alavi. Krill herd: A new bio-inspired optimization algorithm. *Communications in Nonlinear Science and Numerical Simulation*, 17(12):4831 – 4845, 2012. doi: 10.1016/j.cnsns.2012.05.010.

[50] S. Mirjalili, S. M. Mirjalili, and A. Lewis. Grey wolf optimizer. *Advances in Engineering Software*, 69: 46 – 61, 2014. doi: 10.1016/j.advengsoft.2013.12.007.

[51] S. Mirjalili. The ant lion optimizer. *Advances in Engineering Software*, 83:80 – 98, 2015. doi: 10.1016/j.advengsoft.2015.01.010.

[52] J. Xue, Y. Wu, Y. Shi, and S. Cheng. Brain storm optimization algorithm for multi-objective optimization problems. volume 7331, pages 513–519, 06 2012. doi: 10.1007/978-3-642-30976-2_62.

[53] S. Mirjalili. Moth-flame optimization algorithm: A novel nature-inspired heuristic paradigm. *Knowledge-Based Systems*, 89:228 – 249, 2015. doi: 10.1016/j.knosys.2015.07.006.

[54] S. Mirjalili and A. Lewis. The whale optimization algorithm. *Advances in Engineering Software*, 95: 51 – 67, 2016. doi: 10.1016/j.advengsoft.2016.01.008.

[55] S. M. Almufti. Historical survey on metaheuristics algorithms. *International Journal of Scientific World*, 7(1):1, 2019. doi: 10.14419/ijsw.v7i1.29497.

[56] I. Fister, X. S. Yang, J. Brest, and D. Fister. A brief review of nature-inspired algorithms for optimization. *Elektrotehniski Vestnik/Electrotechnical Review*, 80(3):116–122, 2013.

[57] E. Cuevas, M. Cienfuegos, D. Zaldívar, and M. Pérez-Cisneros. A swarm optimization algorithm inspired in the behavior of the social-spider. *Expert Systems with Applications*, 40(16):6374 – 6384, 2013. ISSN 0957-4174. doi: 10.1016/j.eswa.2013.05.041.

[58] O. Abedinia, N. Amjady, and A. Ghasemi. A new metaheuristic algorithm based on shark smell optimization. *Complexity*, 21(5):97–116, 2016. doi: 10.1002/cplx.21634.

[59] M. M. Eusuff and K. E. Lansey. Optimization of water distribution network design using the shuffled frog leaping algorithm. *Journal of Water Resources Planning and Management*, 129(3):210–225, 2003. doi: 10.1061/(ASCE)0733-9496(2003)129:3(210).

[60] H. Shayanfar and F. S. Gharehchopogh. Farmland fertility: A new metaheuristic algorithm for solving continuous optimization problems. *Applied Soft Computing*, 71:728 – 746, 2018. doi: 10.1016/j.asoc.2018.07.033.

[61] A. Mozaffari, A. Fathi, and S. Behzadipour. The great salmon run: a novel bio-inspired algorithm for artificial system design and optimisation. *International Journal of Bio-Inspired Computation (IJBIC)*, 4(5):286–301, 2012. doi: 10.1504/IJBIC.2012.049889.

[62] R. Rivello. *Theory and Analysis of Flight Structures*. McGraw-Hill series in aeronautical and aerospace engineering. McGraw-Hill, 1969. ISBN: 9780070529854.

[63] J. N. Reddy. *Mechanics of Laminated Composite Plates and Shells: Theory and Analysis, Second Edition*. CRC Press, 2 edition, 2003. ISBN: 9780849315923.

[64] J. H. Tam, Z. C. Ong, Z. Ismail, B. C. A. , and S. Y. Khoo. Identification of material properties of composite materials using nondestructive vibrational evaluation approaches: A review. *Mechanics of Advanced Materials and Structures*, 24(12):971–986, 2017. doi: 10.1080/15376494.2016.1196798.

[65] A. L. Araújo, C. M. Soares, and M. M. de Freitas. Characterization of material parameters of composite plate specimens using optimization and experiemental vibrational data. *Composites*, Part B(27B):185–191, 1996. doi: 10.1016/1359-8368(95)00050-X.

[66] J. S. Arora. *Introduction to Optimum Design*. Elsevier, 4^{th} edition, 2004. ISBN: 978-0-12-800806-5.

[67] M. Wahde. *Biologically Inspired Optimization Methods*. WIT, 2008. ISBN: 1845641485.

[68] MATLAB Optimization Toolbox. Matlab optimization toolbox, 2019. The MathWorks, Natick, MA, USA.

[69] R. Sahoo, D. Ojha, and S. Das. Nature inspired metaheuristic algorithms- a comparative review. *International Journal of Development Research*, 6:8427–8432, 07 2016.

[70] S. Mirjalili. Grey wolf optimizer (gwo). MATLAB Central File Exchange, 2020. https://www.mathworks.com/matlabcentral/fileexchange/44974-grey-wolf-optimizer-gwo.

[71] X.-S. Yang. Firefly algorithm. MATLAB Central File Exchange, 2020. https://www.mathworks.com/matlabcentral/fileexchange/29693-firefly-algorithm.

[72] X.-S. Yang. The standard cuckoo search (cs). MATLAB Central File Exchange, 2020. https://www.mathworks.com/matlabcentral/fileexchange/74767-the-standard-cuckoo-search-cs.

[73] D. Larsson. Using modal analysis for estimation of anisotropic material constants background of proposed modal test method. *Journal of Engineering Mechanics*, 123(9–10):222–229, 1997. report.

[74] F. Igea and A. Cicirello. Part-to-part variability assessment of material properties for flat thin orthotropic rectangular panels using Chladni patterns. *Mechanical Systems and Signal Processing*, 139, 2020. doi: 10.1016/j.ymssp.2019.106559.

[75] ANSYS® mechanical apdl 2020 r1 - theory reference. ansyshelp.ansys.com/, 2020.

[76] ANSYS® mechanical apdl 2020 r1 - ansys parametric design language guide. ansyshelp.ansys.com/, 2020.

[77] J. H. Tam. Identification of elastic properties utilizing non-destructive vibrational evaluation methods with emphasis on definition of objective functions: a review. *Structural and Multidisciplinary Optimization*, 2020. doi: 10.1007/s00158-019-02433-1.

[78] K. Hussain, M. N. M. Salleh, S. Cheng, and Y. Shi. Metaheuristic research: a comprehensive survey. *Artificial Intelligence Review*, 52, 2019. doi: 10.1007/s10462-017-9605-z.

[79] P. Frederiksen. Identification of material parameters in anisotropic plates-a combined numerical/-experimental method. *DCAMM Report S*, 60, 1992.

[80] S. Lechnickij, S. Lekhnitskiĭ., J. Brandstatter, and P. Fern. *Theory of Elasticity of an Anisotropic Elastic Body*. Holden-Day series in mathematical physics. Holden-Day, 1963.

[81] M. McIntyre and J. Woodhouse. On measuring the elastic and damping constants of orthotropic sheet materials. *Acta Metallurgica*, 36(6):1397 – 1416, 1988. ISSN 0001-6160. doi: 10.1016/0001-6160(88)90209-X.

[82] R. F. S. Hearmon and A. A. Maradudin. An Introduction to Applied Anisotropic Elasticity. *Physics Today*, 14(10), Jan. 1961. doi: 10.1063/1.3057153.

Appendices

Appendix A

APDL input file (example)

```
    /CLEAR,START
!*********************************Preprocessor*****************************
/PREP7
!*******************************************************************************
!*******************************************************************************
!DimData
Xm =            0.193
Ym =            0.281
thickness =     0.00194
Density =       2688
Nply =          1
plythick =      thickness/Nply
!------------------------------
!Elastic constants!!
EXX =           68.7e9      ! E1
!EYY =           68.1e9    ! E2
!GXY =           24.6e9    ! G12
!GYZ =           26.9e9    ! G23
!GXZ =           26.9e9    ! G13 = G23
vXY =           0.34    ! v12
!----------------
!Numberdivisions
NdivY= 13
NdivX= 9
!----------------------------
Nmodes =20
!!!!!!!!!!!!!!!!!!!!IF NEEDED
!FBlow =20 ! Frequency Boundary Low (Hz)
!FBhigh =1050 ! Frequency Boundary Hight (Hz)
```

```
!*********************************Element Type **********************
ET,1,SHELL63
!*
KEYOPT,1,1,0
KEYOPT,1,3,0
KEYOPT,1,5,0
KEYOPT,1,8,0
KEYOPT,1,9,0
KEYOPT,1,10,0
KEYOPT,1,11,0
!*
!************************Material Properties**************************
!*
R,1,thickness
MPTEMP,1,0
MPDATA,EX,1,,EXX
!MPDATA,EY,1,,EYY
!MPDARA,GXY,1,,GXY
!MPDARA,GYZ,1,,GYZ
!MPDARA,GXZ,1,,GXZ
MPDATA,PRXY,1,,vXY
MPTEMP,1,0
MPDATA,DENS,1,,Density
!*********************************Section*****************************
sect,1,shell,,sp1
secdata, plythick,1,0.0,3
secoffset,MID
seccontrol,,,, , , ,
SECPLOT,   1,,,
!*********************************modelling*****************************
!***********************keypoints*****************************
K, ,,,,
K, ,Xm,,,
K, ,Xm,Ym,,
K, ,,Ym,,
!**********************lines**********************
L,       1,       2
L,       2,       3
L,       3,       4
```

```
L,       4,       1
!*************************************Area*******************************
FLST,2,4,4
FITEM,2,1
FITEM,2,2
FITEM,2,3
FITEM,2,4
AL,P51X
!*****************************************Meshing**********************
FLST,5,2,4,ORDE,2
FITEM,5,2
FITEM,5,4
CM,_Y,LINE
LSEL, , , ,P51X
CM,_Y1,LINE
CMSEL,,_Y
!*
LESIZE,_Y1, , ,NdivY, , , , ,1  !Ndivisions yaxis
!*
FLST,5,2,4,ORDE,2
FITEM,5,1
FITEM,5,3
CM,_Y,LINE
LSEL, , , ,P51X
CM,_Y1,LINE
CMSEL,,_Y
!*
LESIZE,_Y1, , ,NdivX, , , , ,1  !Ndivisions Xaxis
!*
MSHAPE,0,2D
MSHKEY,1
!*
CM,_Y,AREA
ASEL, , , ,       1
CM,_Y1,AREA
CHKMSH,'AREA'
CMSEL,S,_Y
!*
AMESH,_Y1
```

```
!*
CMDELE,_Y
CMDELE,_Y1
CMDELE,_Y2

!*************************************Solution****************
FINISH
/SOL
!*********************************Analysis Type**********
ANTYPE,2 !MODAL analysis
!****************Options*****************
MODOPT,LANB,Nmodes   !# modes
EQSLV,SPAR
MXPAND,Nmodes, , ,0
LUMPM,0
PSTRES,0
!*
!MODOPT,LANB,FBlow,0,FBhigh, ,OFF  !frequency boundaries
/STATUS,SOLU
! SOLVE
/STATUS,SOLU
SOLVE
FINISH
/POST1
SET,LIST
```

Appendix B

Convergence of element SHELL181

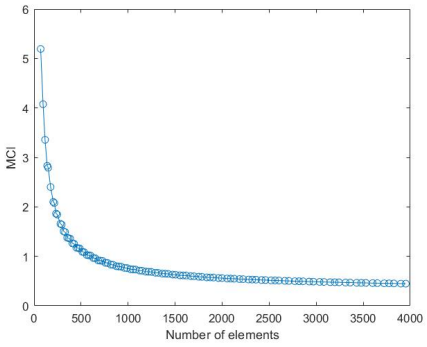

(a) SP-1

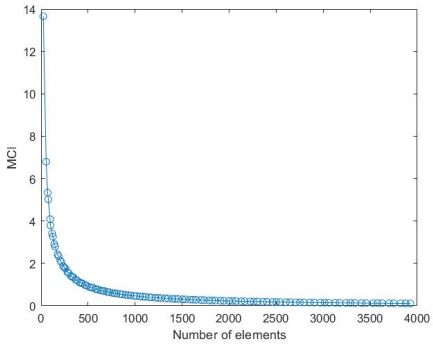

(b) SP-3

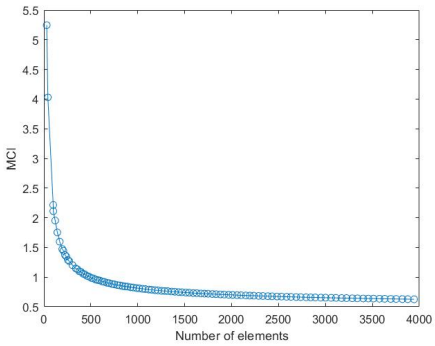

(c) SP-5

Figure B.1: Convergence for element type SHELL181

Appendix C

Results computed with different sets of search agents

Table C.1: Computational time, objective function function value, the elastic constants computed and the iteration for each one of the fifty runs and the extreme cases (initial populations at the bounds for the design variables) performed for the SP-1

Optimisation number	Computational time (h)	Function value	E(GPa)	ν	Iterations
1	1.094	72.75	66.82	0.3759	60
2	1.025	72.75	66.82	0.3759	56
3	0.969	72.75	66.82	0.3759	53
4	0.883	72.75	66.82	0.3759	48
5	0.908	72.75	66.82	0.3759	49
6	1.082	72.75	66.82	0.3759	59
7	1.285	72.75	66.82	0.3759	48
8	0.898	72.75	66.82	0.3759	49
9	1.097	72.75	66.82	0.3759	59
10	1.011	72.75	66.82	0.3759	54
11	1.040	72.75	66.82	0.3759	57
12	0.841	72.75	66.82	0.3759	46
13	1.090	72.75	66.82	0.3759	60
14	0.892	72.75	66.82	0.3759	49
15	1.074	72.75	66.82	0.3759	59
16	1.147	72.75	66.82	0.3759	63
17	1.016	72.75	66.82	0.3759	56
18	1.111	72.75	66.82	0.3759	61
19	1.001	72.75	66.82	0.3759	55
20	1.149	72.75	66.82	0.3759	63
21	1.061	72.75	66.82	0.3759	58
22	1.046	72.75	66.82	0.3759	57
23	0.877	72.75	66.82	0.3759	48
24	0.904	72.75	66.82	0.3759	49
25	1.083	72.75	66.82	0.3759	59
26	0.990	72.75	66.82	0.3759	54
27	1.039	72.75	66.82	0.3759	57
28	0.836	72.75	66.82	0.3759	46
29	1.094	72.75	66.82	0.3759	60
30	0.892	72.75	66.82	0.3759	49
31	1.080	72.75	66.82	0.3759	59
32	1.149	72.75	66.82	0.3759	63
33	1.023	72.75	66.82	0.3759	56
34	1.114	72.75	66.82	0.3759	61
35	1.004	72.75	66.82	0.3759	55
36	1.152	72.75	66.82	0.3759	63
37	1.060	72.75	66.82	0.3759	58
38	1.041	72.75	66.82	0.3759	57
39	1.006	72.75	66.82	0.3759	55
40	1.227	72.75	66.82	0.3759	67
41	1.048	72.75	66.82	0.3759	57
42	1.330	72.75	66.82	0.3759	72
43	1.118	72.75	66.82	0.3759	61
44	1.061	72.75	66.82	0.3759	58
45	1.128	72.75	66.82	0.3759	62
46	1.078	72.75	66.82	0.3759	59
47	1.080	72.75	66.82	0.3759	59
48	1.182	72.75	66.82	0.3759	65
49	1.135	72.75	66.82	0.3759	62
50	1.128	72.75	66.82	0.3759	61
51*	1.268	72.75	66.82	0.3759	69
52**	1.233	72.75	66.82	0.3759	68

*Initial population at the lower bounds of the design variables; **Initial population at the upper bounds of the design variables.

Table C.2: Time, function value, iteration and elastic constants computed in each one of the thirty runs performed for the SP-2

Optimisation number	Computational time (h)	Function value	E_1(GPa)	E_2(GPa)	G_{12}(GPa)	ν_{12}	Iterations
1	6.863	45.66	30.51	27.15	6.38	0.1674	139
2	11.614	45.69	30.51	27.15	6.40	0.1672	213
3	12.103	45.67	30.51	27.15	6.38	0.1673	215
4	9.989	45.65	30.51	27.15	6.38	0.1674	183
5	15.139	45.67	30.51	27.15	6.38	0.1673	258
6	7.544	45.65	30.51	27.15	6.38	0.1674	140
7	8.203	45.68	30.51	27.15	6.39	0.1672	165
8	9.366	45.68	30.51	27.15	6.39	0.1672	185
9	13.551	45.67	30.51	27.15	6.39	0.1673	261
10	13.376	45.64	30.52	27.15	6.37	0.1674	228
11	11.117	45.67	30.51	27.15	6.39	0.1673	210
12	18.267	45.65	30.51	27.15	6.37	0.1674	324
13	12.787	45.65	30.51	27.15	6.37	0.1674	234
14	8.096	45.66	30.51	27.15	6.38	0.1674	162
15	12.040	45.66	30.51	27.15	6.38	0.1674	227
16	8.250	45.66	30.51	27.15	6.38	0.1673	166
17	11.708	45.66	30.51	27.15	6.38	0.1674	222
18	6.638	45.65	30.51	27.15	6.38	0.1674	138
19	11.928	45.66	30.51	27.15	6.38	0.1673	226
20	20.761	45.65	30.51	27.15	6.37	0.1674	374
21	6.712	45.65	30.51	27.15	6.38	0.1674	143
22	13.403	45.67	30.51	27.15	6.38	0.1673	243
23	16.426	45.65	30.52	27.15	6.37	0.1674	290
24	6.131	45.66	30.51	27.15	6.38	0.1674	134
25	8.293	45.66	30.51	27.15	6.38	0.1674	174
26	13.964	45.68	30.51	27.15	6.39	0.1673	255
27	7.045	45.66	30.51	27.15	6.38	0.1673	146
28	6.285	45.68	30.51	27.15	6.39	0.1673	141
29	11.291	45.66	30.51	27.15	6.38	0.1674	227
30	11.291	45.66	30.51	27.15	6.38	0.1674	227
31*	7.514	45.65	30.51	27.15	6.37	0.1674	145
32**	9.769	45.66	30.51	27.15	6.38	0.1674	181

*Initial population at the lower bounds of the design variables; **Initial population at the upper bounds of the design variables.